Thesis for the Degree of Doctor of Philosophy

On Hard-Decision Forward Error Correction with Application to High-Throughput Fiber-Optic Communications

Alireza Sheikh

CHALMERS

Communication Systems Group
Department of Electrical Engineering
Chalmers University of Technology
Gothenburg, Sweden, 2019

On Hard-Decision Forward Error Correction with Application to High-Throughput Fiber-Optic Communications

Alireza Sheikh

ISBN 978-91-7597-870-3

Doktorsavhandlingar vid Chalmers tekniska högskola
Ny serie nr 4551
ISSN 0346-718X

Communication Systems Group
Department of Electrical Engineering
Chalmers University of Technology
SE–412 96 Gothenburg, Sweden
Phone: +46 (0)31 772 1000
www.chalmers.se

Typeset by the author using LaTeX.

Printed by Chalmers Reproservice
Gothenburg, Sweden, 2019

Abstract

The advent of the Internet not only changed the communication methods significantly, but also the life-style of the human beings. The number of Internet users has grown exponentially in the last decade, and the number of users exceeded 3.4 billion in 2016. Fiber links serve as the Internet backbone, hence, the fast grow of the Internet network and the sheer of new applications is highly driven by advances in optical communications. The emergence of coherent optical systems has led to a more efficient use of the available spectrum compared to traditional on-off keying transmission, and has made it possible to increase the supported data rates.

To achieve high spectral efficiencies and improve the transmission reach, coding in combination with a higher order modulation, a scheme known as coded modulation (CM), has become indispensable in fiber-optic communications. In the recent years, graph-based codes such as low-density parity-check codes and soft decision decoding (SDD) have been adopted for long-haul coherent optical systems. SDD yields very high net coding gains but at the expense of a relatively high decoding complexity, which brings implementation challenges at very high data rates. Hard decision decoding (HDD) is an appealing alternative that reduces the decoding complexity. This motivates the focus of this thesis on forward error correction (FEC) with HDD for high-throughput, low power fiber-optic communications.

In this thesis, we start by studying the performance bounds of HDD. In particular, we derive achievable information rates (AIRs) for CM with HDD for both bit-wise and symbol-wise decoding, and show that bit-wise HDD yields significantly higher AIRs. We also design nonbinary staircase codes using density evolution. Finite length simulation results of binary and nonbinary staircase codes corroborate the conclusions arising from the AIR analysis, i.e., for HDD binary codes are preferable. Then, we consider probabilistic shaping. In particular, we extend the probabilistic amplitude shaping (PAS) scheme recently introduced by Böcherer *et al.* to HDD based on staircase codes. Finally, we focus on new decoding algorithms for product-like codes to close the gap between HDD and SDD, while keeping the decoding complexity low. In particular, we propose three novel decoding algorithms for product-like codes based on assisting the HDD with some level of soft information. The proposed algorithms provide a clear performance-complexity tradeoff. In particular, we show that up to roughly half of the gap between SDD and HDD can be closed with limited complexity increase with respect to HDD.

Keywords: Achievable information rates, bounded distance decoding, coded modulation, generalized minimum distance decoding, hard decision decoding, probabilistic shaping, product codes, product-like codes, staircase codes.

List of Publications

This thesis is based on the work contained in the following appended papers:

Paper A
A. Sheikh, A. Graell i Amat, and G. Liva, "Achievable Information Rates for Coded Modulation with Hard Decision Decoding for Coherent Fiber-Optic Systems," *IEEE/OSA J. Lightw. Technol.*, vol. 35, no. 23, pp. 5069–5078, Dec. 2017.

Paper B
A. Sheikh, A. Graell i Amat, and M. Karlsson, "Nonbinary Staircase Codes for Spectrally and Energy Efficient Fiber-Optic Systems," in *Proc. Optical Fiber Commun. Conf. (OFC)*, Los Angeles, CA, Mar. 2017.

Paper C
A. Sheikh, A. Graell i Amat, G. Liva, and F. Steiner, "Probabilistic Amplitude Shaping with Hard Decision Decoding and Staircase Codes," *IEEE/OSA J. Lightw. Technol.*, vol. 36, no. 9, pp. 1689–1697, May. 2018.

Paper D
A. Sheikh, A. Graell i Amat, and G. Liva, "Binary Message Passing Decoding of Product-like Codes," submitted to *IEEE Trans. Commun.*, Feb. 2019.

Paper E
A. Sheikh, A. Graell i Amat, G. Liva, C. Häger, and H. D. Pfister, "On Low-Complexity Decoding of Product Codes for High-Throughput Fiber-Optic Systems," in *Proc. IEEE Int. Symp. Turbo Codes & Iterative Inf. Processing (ISTC),* Hong Kong, Dec. 2018. **(Invited paper)**

Paper F
A. Sheikh, A. Graell i Amat, and G. Liva, "Binary Message Passing Decoding of Product Codes Based on Generalized Minimum Distance Decoding," in *Proc. 53rd Annu. Conf. Inf. Sciences and Systems (CISS),* Baltimore, MD, Mar. 2019.
(Invited paper)

Other related publications of the author not included in this thesis:

- **A. Sheikh**, C. Fougstedt, A. Graell i Amat, P. Johannisson, P. Larsson-Edefors, and M. Karlsson, "Dispersion Compensation Filter Design Optimized for Robustness and Power Efficiency," in *Proc. Advanced Photonics*, Boston, MA, Jun. 2015.

- C. Fougstedt, **A. Sheikh**, P. Johannisson, A. Graell i Amat, and P. Larsson-Edefors, "Power-Efficient Time-Domain Dispersion Compensation Using Optimized FIR Filter Implementation," in *Proc. Advanced Photonics*, Boston, MA, Jun. 2015.

- **A. Sheikh**, C. Fougstedt, A. Graell i Amat, P. Johannisson, P. Larsson-Edefors, and M. Karlsson, "Dispersion Compensation FIR Filter With Improved Robustness to Coefficient Quantization Errors," *IEEE/OSA J. Lightw. Technol.*, vol. 34, no. 22, pp. 5110-5117, Nov. 2016.

- **A. Sheikh**, A. Graell i Amat, and G. Liva, "On Achievable Information Rates for Coherent Fiber-Optic Systems with Hard Decision Decoding," in *Proc. European Conf. Optical Commun. (ECOC)*, Gothenburg, Sweden, Sep. 2017.

- **A. Sheikh**, A. Graell i Amat, and G. Liva, "Probabilistically-Shaped Coded Modulation with Hard Decision Decoding for Coherent Optical Systems," in *Proc. European Conf. Optical Commun. (ECOC)*, Gothenburg, Sweden, Sep. 2017.

- C. Fougstedt, **A. Sheikh**, P. Johannisson, and P. Larsson-Edefors, "Filter Implementation for Power-Efficient Chromatic Dispersion Compensation," *IEEE Photon. J.*, vol. 10, no. 4, pp. 1-19, Aug. 2018.

- **A. Sheikh**, A. Graell i Amat, and G. Liva, "Iterative Bounded Distance Decoding of Product Codes with Scaled Reliability," in *Proc. European Conf. Optical Commun. (ECOC)*, Rome, Italy, Sep. 2018.

- C. Fougstedt, **A. Sheikh**, A. Graell i Amat, G. Liva, and P. Larsson-Edefors, "Energy-Efficient Soft-Assisted Product Decoders," in *Proc. Optical Fiber Commun. Conf. (OFC)*, San Diego, CA, Mar. 2019.

Acknowledgment

My Phd journey started on Oct. 2014, when I was a bit younger and less experienced. At that time, I never expected how much experience I would get by doing a Phd for the next 4.5 years. In my Phd life, there were joyful times and also moments that I felt really disappointed and frustrated. Overall, I am pleased that I decided to join Chalmers and do a Phd, and now it is a time to gratitude all people helped me over these years.

First and foremost, I would like to express my deepest gratitude to my main supervisor, Prof. Alexandre Graell i Amat for his support, motivation, patience, and guidance. Àlex, thanks for letting me exploring different topics and work on interesting research problems. Next, my heart-felt thanks goes to my unofficial co-supervisor Dr. Gianluigi Liva, for our technical discussions and giving me the opportunity to visit Institute of Communications and Navigation of the German Aerospace Center (DLR), Germany. I wish also to thank my co-supervisor Prof. Magnus Karlsson for all fruitful discussions we had at the beginning of my Phd studies. I would also like to appreciate Prof. Erik Agrell and Prof. Peter Andrekson for their support in my project. I wish also to thank Dr. Alex Alvarado for giving me the opportunity to visit the Eindhoven University of Technology, Netherlands. I am also thankful to Dr. Pontus Johannisson for his guidance in the first year of my PhD.

I would also like to thank the head of the communication and antenna systems (CAS) division, Prof. Erik Ström for providing an awesome work place. Special thanks to Agneta and Rebecka for helping with the administrative works. Thanks in general to all former and current members of the CAS and fiber-optic communications research centre. In particular, many thanks to Christoffer, Dr. Christian Häger, Dr. Naga V. Irukulapati, Dr. Chayan Bhar, and Dr. Houman Rastegarfar. A special thank to my office mate Kamran, for all the technical and nontechnical discussions we had. Thanks Mohammad for helping me accessing my PC in Chalmers, during my research visits. I had a great time, being surrounded by my great friends in the large Iranian community at Chalmers. Thanks all for making me feel at home.

My outmost gratitude goes to my precious family, especially my parents and my brother, for your support and encouragement in all steps of my life.

Last but not least, I deeply gratitude my wife, Shayesteh, for her kindness, patience, and motivation. Thanks for enduring my nagging about Phd :) .

Finally, I would like to finish with a Persian poem, reminding me some good

memories:

زندگی صحنه ی یکتای هنرمندی ماست هر کسی نغمه خود خواند و از صحنه رود

صحنه پیوسته به جا است...

خرم آن نغمه که مردم بسپارند به یاد

ژاله اصفهانی

Translation: Life is a unique artistry scene, everybody sings his/her own song and finally leaves the scene, but the scene is always there..., the prosperous song is the one that people remember (Zhale Esfahani).

Alireza Sheikh
Gothenburg, April 2019

Financial support

This work was funded by the Knut and Alice Wallenberg Foundation. I would also like to thank Ericsson's Research Foundation for partially supporting my research visit in the Institute of Communications and Navigation of the German Aerospace Center (DLR), Germany. The simulations were performed in part on resources at the Chalmers Centre for Computational Science and Engineering (C3SE) provided by the Swedish National Infrastructure for Computing (SNIC).

Acronyms

AD Anchor Decoding

AIR Achievable Information Rate

ASE Amplified Spontaneous Emission

AWGN Additive White Gaussian Noise

BCH Bose-Chaudhuri-Hocquenghem

BDD Bounded Distance Decoding

BER Bit Error Rate

BICM Bit-Interleaved Coded Modulation

BMP-GMDD Binary Message Passing based on Generalized Minimum Distance Decoding

CCDM Constant Composition Distribution Matching

CD Chromatic Dispersion

CM Coded Modulation

CN Constraint Node

DBP Digital Back Propagation

DE Density Evolution

DMC Discrete Memoryless Channel

DS Direct Sampling

DSP Digital Signal Processing

EDFA Erbium-Doped Fiber Amplifier

FEC Forward Error Correction

FOC Fiber-Optic Channel

GLDPC Generalized Low-Density Parity-Check

GN Gaussian Noise

GVD Group Velocity Dispersion

HdChaD Hard detector/Channel-aware Decoder

HdChaD-BW Bit-Wise Hard detector/Channel-aware Decoder

HDD Hard Decision Decoding

HD FEC Hard Decision Forward Error Correction

iBDD iterative Bounded Distance Decoding

iBDD-SR iterative Bounded Distance Decoding with Scaled Reliability

iGMDD-SR iterative Generalized Minimum Distance Decoding with Scaled Reliability

LDPC Low-Density Parity-Check

LS-BL Least-Squares Band-Limited

LS-CO Constrained Least-Squares

NLSE Nonlinear Schrödinger Equation

OH Overhead

PAS Probabilistic Amplitude Shaping

PC Product Code

Pdf Probability density function

PMD Polarization Mode Dispersion

PSD Power Spectral Density

QAM Quadrature Amplitude Modulation

QSC Q-ary Symmetric Channel

RS Reed Solomon

RV Random Variable

SC-LDPC	Spatially Coupled Low-Density Parity-Check
SDD	Soft Decision Decoding
SMF	Single Mode Fiber
SNR	Signal-to-Noise Ratio
SOP	State-of-Polarization
SSFM	Split Step Fourier Method
TPD	Turbo Product Decoding
VN	Variable Node
WDM	Wavelength-Division Multiplexing

Contents

Part I

Introductory Chapters

Chapter 1

Introduction

Probably most of the people who use their cell phones daily, send emails, chat with their friends via different applications, watch movies online, and use social media networks, do not recognize that in a way, their messages are transformed into photons somewhere and transmitted through fiber-optic links. Optical fibers are used as the Internet backbone and to a less extend as the backhaul network in wireless communications. The communication distance in optical systems varies from few meters in data centers to thousands of kilometers for transoceanic links. Compared to wireless communication, optical communication has the benefit of unlicensed transmission without electromagnetic interference. For transmission over long distances with high aggregated data rates, optical communication is the most prevalent communication method since optical fibers yield substantially lower loss compared to other communication mediums.

Traditionally, optical communication was based on on-off keying modulation at the transmitter and power detection at the receiver. The advent of erbium-doped fiber amplifiers (EDFAs) [1, 2] along with lasers with narrow line-width enabled the emergence of coherent optical communications. These technical developments boosted the data rates from 1 Gb/s in the mid-1980s to 1 Tb/s in early 2000s [3]. Coherent optical systems increase the spectral efficiency by modulating the data in both the in-phase and quadrature components of the optical field. The spectral efficiency can be increased further by using two polarizations jointly, taking the interaction between polarizations into account using digital signal processing (DSP) at the receiver.

The long transmission distance along with high data rates makes it impossible to employ retransmission schemes in optical communications. Therefore, an stringent 10^{-15} bit error rate (BER) requirement on the decoded data is set to ensure the quality of data transmission, which in turn makes forward error correction (FEC) indispensable for fiber-optic communications [4]. In theory, one can operate at arbitrarily low BER if the data rate is lower than the so-called *Shannon limit* [5]. In practice, however, operating at low BER and close to Shannon limit is at the expense

Figure 1.1: The components of the DSP of a coherent fiber-optic system.

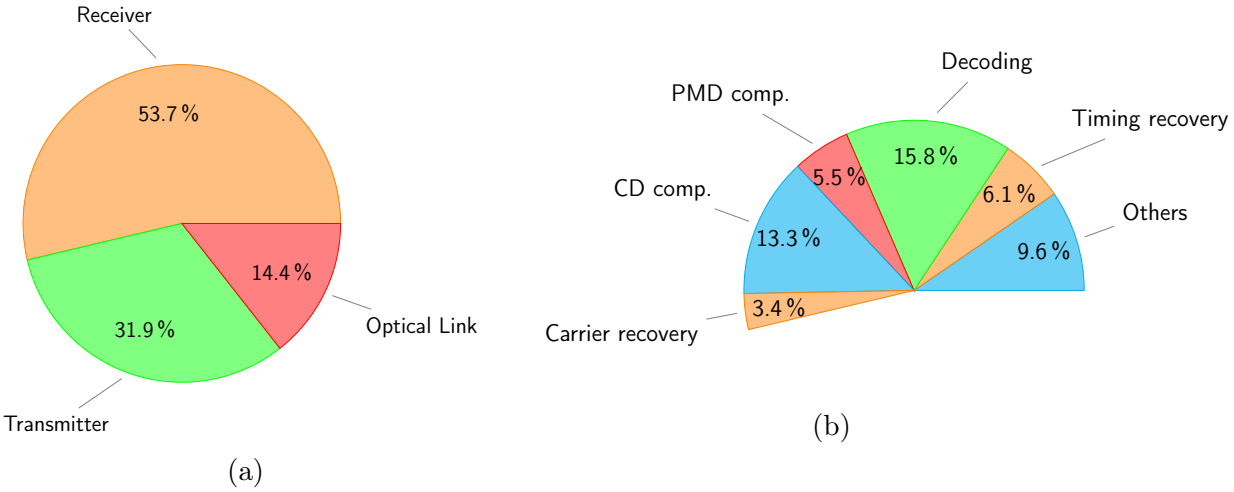

Figure 1.2: (a) The energy consumption (in percentage) of different components of a coherent fiber-optic system for a 2400 km link with lumped amplification and 16-QAM modulation. Data is extracted from [7, Table XVI]. (b) The energy consumption (in percentage) of the receiver components.

of increased system complexity. Therefore, FEC design is a nontrivial task of finding new coding schemes by considering the trade-offs between system performance and complexity. Optical systems are typically operated at hundreds of Gigabit-per-second, and designing a low-complex decoder operating at such high data rate is a tricky task [6]. Soft decision decoding (SDD) can operate close to the Shannon limit, but it entails relatively high decoding complexity and data flow. This makes adapting SDD for high-throughput applications very challenging. Hard decision decoding (HDD) is an appealing alternative due to its associated low decoding data flow. In this thesis, our focus is primarily on proposing new coding schemes based on HDD with constrained complexity to improve the performance of the system.

In fiber-optic communications, several impairments, such as chromatic dispersion (CD), fiber loss, nonlinearity, and polarization mode dispersion (PMD), deteriorate the transmitted signal. These impairments must be compensated for in the DSP block of the receiver. Coherent transmission enables using sophisticated DSP methods to improve the system performance which in turn leads to extending the transmission reach. However, using more complex algorithms in the DSP results in an increased energy consumption. Several studies have addressed the estimation of the energy consumption of coherent optical systems and several implementations have been proposed [7–11]. The main components of the DSP block of the receiver are shown in Fig. 1.1. In the CD compensation component, the accumulated CD due to

the group velocity dispersion (GVD) is compensated for [12]. The timing recovery block synchronizes the sampling time at the receiver and can be implemented based on data-aided or blind algorithms [13]. The PMD is usually compensated by an adaptive filter using well-known algorithms such as constant composition or radius directed equalization [14, 15]. The carrier recovery, which is due to the frequency and phase mismatch between the input signal and the local oscillator, is compensated for using the Viterbi-and-Viterbi algorithm [16]. The energy consumption of the decoder highly varies based on the code used and the implementation details. In general, SDD is significantly more energy-hungry than HDD. Fig. 1.2 summarizes the energy consumption of different components of the coherent optical link as well as different components of the receiver DSP for a case study given in [7]. In this case study, the data, of length 20489 bits, is encoded by a low-density parity-check (LDPC) code with SDD and code length of 24576 bits [17], and transmitted over a 2400 km link with lumped amplification using quadrature amplitude modulation (QAM) with order of 16. Fig. 1.2(a) summarizes the portion of the overall energy consumption corresponding to the transmitter, optical amplifiers, and receiver. As can be seen, the receiver is the most energy-hungry. In Fig. 1.2(b), the energy consumption of the different components of the receiver is shown. One can see that the decoder is the major energy-hungry block. This highlights the need for proposing new coding schemes with lower complexity to boost the energy efficiency of the overall receiver.

Several FEC schemes based on SDD have been proposed for fiber-optic channels [18–28]. In particular, block-turbo codes with highly parallelized suboptimal SDD of the component codes based on the Chase-Pyndiah decoder has been shown to provide large net coding gains [18]. Binary LDPC codes are another popular SDD-based class of codes for the fiber-optic channel [19–24]. However, LDPC codes suffer from an error floor and usually are concatenated with high rate outer algebraic codes to remove the floor [4]. Nonbinary LDPC codes have also been considered for optical systems, but the associated complexity is high [25]. Recently, spatially coupled LDPC (SC-LDPC) codes have also been investigated for optical systems [26–28]. In particular, SC-LDPC codes have been shown to provide promising net coding gains with feasible implementation complexity [26]. In general, SDD provides high net coding gain while entails high decoding data flow and memory requirements [29]. Although there is a research line on reducing the complexity of SDD [30–33], an alternative is resorting to HDD. HDD reduces the decoder data flow, at the cost of some performance loss compared to SDD [29]. Historically, high rate Bose-Chaudhuri-Hocquenghem (BCH) or Reed Solomon (RS) codes have been used in fiber-optic communications to meet the BER requirements. More precisely, the RS(255,239) code with an interleaver of depth 16 was used to meet the required output BER of 10^{-12} with a channel BER threshold of approximately 2×10^{-4} [34]. Several concatenated structures based on HDD have also been considered in the optical submarine standard [35]. Product-like

codes are a family of linear block codes built from shorter component (block) codes, where each code bit is protected by more than one component code. Component codes are typically RS or BCH codes, which can be efficiently decoded via algebraic bounded distance decoding (BDD). Product codes (PCs) originally introduced in 1958 by Peter Elias [36] are the original member of this family. For 2-dimensional PCs each code bit is protected by two component codes and each codeword can be represented accordingly by a two-dimensional rectangular array. Recently, HDD of product-like codes such as PCs, half PCs [37], braided codes [38], staircase codes [29], and other product-like codes [39] based on BDD of the component codes has gained attention in the optical community due to its excellent performance–complexity tradeoff.

In this thesis, our focus is on HDD of product-like codes and coded modulation (CM) schemes thereof. Our goal is to propose new coding schemes that outperform the state-of-the-art HDD schemes with reasonable implementation complexity, in order to achieve very high throughputs and low power consumption. To shed light on the performance bounds of HDD systems, in Paper A we derive the achievable information rates (AIRs) of binary and nonbinary codes with HDD. In particular, we consider a conventional CM system where after hard detection, the decoder operates solely based on the Hamming distance metric [29,36–38]. We show that binary codes provide higher AIRs than their nonbinary counterpart under HDD. The conclusion of Paper A is interesting, since the decoder of nonbinary codes is generally more complex than that of binary codes, therefore, Paper A suggests that one needs to only consider binary codes for HDD. The AIR is a limit for infinitely long block-length codes. To corroborate the results of Paper A for finite length codes, we consider the design of nonbinary staircase codes and compare their resulting spectral efficiency with that of binary staircase codes for different overheads (OHs). Binary staircase codes can be optimized for different OHs using Monte-Carlo simulations [40] or density evolution (DE) analysis [41]. Motivated by [41], in Paper B, we derive the DE for SC-GLDPC ensemble with RS component codes, and then, we optimize the component code parameters of the nonbinary staircase code. By comparing the performance of binary and nonbinary staircase codes in Paper A, the conclusion drawn from the AIR analysis is corroborated.

Constellation shaping is a method to improve the performance of CM systems and reduce the shaping-loss due to the use of a conventional constellation with equidistant signal points and uniform signaling. In particular, geometric shaping [42–46] and probabilistic shaping [47–49] have been proposed in the literature. Recently, probabilistic amplitude shaping (PAS) with SDD [49] has become popular in the optical community due to its structured system model and excellent performance, which can be implemented with off-the-shell constellations. In paper C, we extend the PAS concept to a CM system with HDD and staircase codes. We show that using PAS with staircase codes one can operate within 0.57–1.44 dB of the corresponding AIR. Furthermore, gains up to 2.88 dB are observed compared to the conventional CM

with HDD.

Product-like codes are typically decoded using iterative BDD of the component codes. BDD does not employ the channel reliabilities in decoding and can be implemented efficiently using the Berlekamp-Massey algorithm [50, 51]. In papers D and E, we propose novel decoding algorithms for product-like codes, called iBDD-SR and iGMDD-SR, which employ the channel reliabilities selectively in iterative BDD of the component codes. In particular, in Paper D, we derive a DE analysis for both GLDPC and SC-GLDPC ensembles decoded using iBDD-SR. Based on the derived DE, we optimize the design parameter of iBDD-SR for both PCs and staircase codes. We show that gains up to 0.29 dB and 0.31 dB compared to conventional iterative BDD can be achieved for PCs and staircase codes, respectively. Furthermore, we evaluate the complexity of iBDD-SR and show that these extra gains are at the cost of limited increase in decoding complexity and some extra memory in the decoder. We also implement iBDD-SR for PCs and show that a PC decoded using iBDD-SR can achieve the performance of a staircase code with the same OH and conventional iterative BDD, with less than half area and energy dissipation [52]. Furthermore, we show that up to 1 Tbps can be achieved with only a small increase in energy per information bit compared to iterative BDD. In Paper E, we propose the iGMDD-SR algorithm that can further improve the performance at the expense of higher internal data flow of the iterative decoder. In particular we show that iGMDD-SR reduces the gap between iterative BDD and SDD based on Chase-Pyndiah algorithm [18] by more than 50%. In Paper F, we propose a new decoding algorithm, called BMP-GMDD, for PCs by modifying the iGMDD-SR algorithm to reduce the internal data flow. We show that BMP-GMDD closes roughly half of the gap between iterative BDD and SDD based on the Chase-Pyndiah algorithm with significantly lower data flow compared to iGMDD-SR. We also show that the excellent performance of BMP-GMDD over iterative BDD is at the cost of a minor additional data flow (in the order of 8% to 30% depending on the component codes). Therefore, BMP-GMDD provides an excellent performance–complexity tradeoff.

1.1 Organization of the Thesis

A PhD thesis in Sweden can be written either as a monograph or a collection of papers. The format of this thesis is a collection of papers. It is divided into two parts: the first part provides the reader the background necessary for understanding the second part, i.e., the research papers. The intended audience of the thesis are graduate students and researchers currently working or planning to work in optical communications, who have some background in coding theory and digital communications.

The rest of the thesis is organized as follows. In Chapter 2, we briefly discuss signal propagation across the fiber and the corresponding impairments. Then, we explain the numerical method to emulate fiber propagation. The chapter is concluded by

reviewing the fiber-optic channel modeling. In Chapter 3, we review some basics about CM. Then, PCs and staircase codes as two powerful codes based on HDD are introduced. The chapter is concluded by introducing the DE concept as an analytical tool for designing the code parameters. In Chapter 4 PAS as a way to induce the capacity-achieving distribution in a CM system is briefly explained. The chapter follows by reviewing iterative BDD as a conventional decoding method for product-like codes and also new proposals to improve the decoding performance with respect to iterative BDD. Finally, Chapter 5 serves as a brief description of Part II, which contains the appended papers.

1.2 Notation

The following notation is used throughout the thesis. We denote by $p_X(\cdot)$ the probability mass function (pmf) or the probability density function (pdf) of a (discrete or continuous) random variable (RV) X. $P_{Y|X}(Y|X)$ denotes the pdf of the RV Y conditioned on X. Unless otherwise specified, we use boldface letters to denote vectors and matrices, e.g., $\boldsymbol{x}$ and $\boldsymbol{X}$, respectively. Expectation with respect to the pmf or pdf of RV X is denoted by $\mathbb{E}_X(\cdot)$. $\exp(\cdot)$ denotes the exponential function. $(\cdot)^{\mathsf{T}}$ and $(\cdot)^{\mathsf{H}}$ stand for the transpose and hermitian conjugate operations, respectively. $|\cdot|$ gives the absolute value while $\lfloor x \rfloor$ gives the greatest integer less than or equal to x. Furthermore, calligraphic letters are used for sets.

Chapter 2

Fiber-Optic Communication Systems

The optical fiber consists of a cylindrical core made of silica glass that is surrounded by a cladding layer. The cladding layer has a lower refractive index than the fiber core, which leads to guiding the light along the main axis of the fiber. This phenomenon is called *internal reflection* [53]. The propagation of the light inside the fiber can be examined by solving Maxwell's equations. Each solution of Maxwell's equations satisfying the boundary conditions of the fiber is called a *propagation mode* of the fiber. Fibers with more than one mode are used for noncoherent transmission and short distance applications such as transmission in data centers. On the contrary, single mode fibers (SMFs) have only one propagation mode, known as the *fundamental mode*, and are used mainly in long-haul coherent optical systems. Although SMFs provide much lower loss compared to copper wires, hence enabling the extension of the transmission reach, amplifiers are still required for transmission over long distances. Amplifiers add noise to the original signal, leading to the so-called *signal-noise interaction* phenomenon during propagation. Optical fiber impairments such as GVD and Kerr-nonlinearity also distort the transmitted signal.

In this thesis, we consider high-throughput, low-power fiber-optic systems. In order to design the FEC, a channel model for signal propagation is required. A channel model is a mathematical description of the relation between input and output, which in general depends on the propagation environment and possibly the components of the transmitter (e.g., laser, encoder, etc) and receiver (e.g. equalizer, filters, etc). In this chapter, we briefly review the impairments associated with signal transmission in the fiber, numerical methods to emulate propagation in the fiber, and the corresponding channel modeling.

2.1 Signal Propagation in Fiber-Optic Channels

Propagation of a single-polarized (X-polarization) signal over a fiber-optic channel can be described by the nonlinear Schrödinger equation (NLSE). The NLSE is a

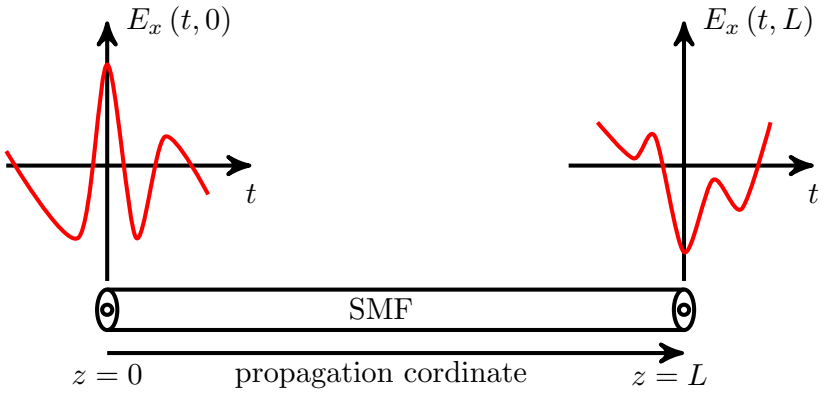

Figure 2.1: Schematic of transmission over a SMF with input $E_x(t,0)$ and output $E_x(t,L)$. The NLSE gives the mathematical relation between $E_x(t,0)$ and $E_x(t,L)$.

mathematical description of the input-output given as

$$\frac{\partial E_x(t,z)}{\partial z} - i\gamma|E_x(t,z)|^2 E_x(t,z) + i\frac{\beta_2}{2}\frac{\partial^2 E_x(t,z)}{\partial t^2} + \frac{\alpha}{2}E_x(t,z) = 0, \tag{2.1}$$

where $E_x(t,z)$ is the envelope of the optical field, γ is the nonlinear coefficient, β_2 is the GVD parameter, α is the loss parameter, z is the propagation distance, and t is the time coordinate moving with a speed corresponding to the group velocity of the signal. Fig. 2.1 shows a schematic of transmission over a SMF with input $E_x(t,0)$ and output $E_x(t,L)$. One can increase the spectral efficiency of the system by transmitting a signal in the "Y-polarization" simultaneously. Propagation over two polarizations implies that interactions between polarizations should be taken into account. Since the polarization state changes rapidly, it can be shown that the propagation of different polarizations averaged over fast changing polarization states can be described by the Manakov equation [54, 55],

$$\frac{\partial \boldsymbol{E}(t,z)}{\partial z} - i\gamma\frac{8}{9}||\boldsymbol{E}(t,z)||^2\boldsymbol{E}(t,z) + i\frac{\beta_2}{2}\frac{\partial^2 \boldsymbol{E}(t,z)}{\partial t^2} + \frac{\alpha}{2}\boldsymbol{E}(t,z) = 0, \tag{2.2}$$

where $\boldsymbol{E} \triangleq [E_x, E_y]^{\mathsf{T}}$ is a vector containing the field envelopes in the two polarizations, and $||\boldsymbol{E}(t,z)||^2 \triangleq \boldsymbol{E}^{\mathsf{H}}\boldsymbol{E}$. One can see (2.2) as two coupled equations for the two polarizations. In the following, we explain different fiber impairments, described by both the Schrödinger and Manakov equations, in more detail.

2.1.1 Fiber Loss and Amplifier Noise

If we neglect the dispersion and nonlinearity, i.e., $\beta_2 = \gamma = 0$, the Manakov equation has the closed-form solution

$$\boldsymbol{E}(t,z) = \boldsymbol{E}(t,0)\exp(-\alpha z/2). \tag{2.3}$$

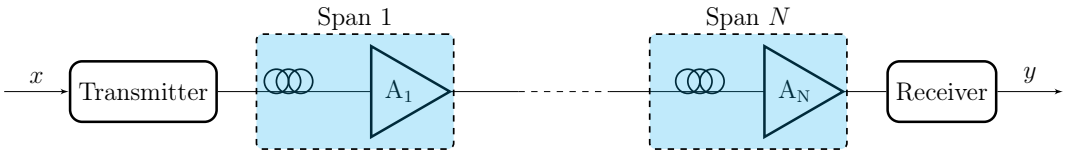

Figure 2.2: A fiber-optic link with N spans, input x and output y. Each span consists of an amplifier.

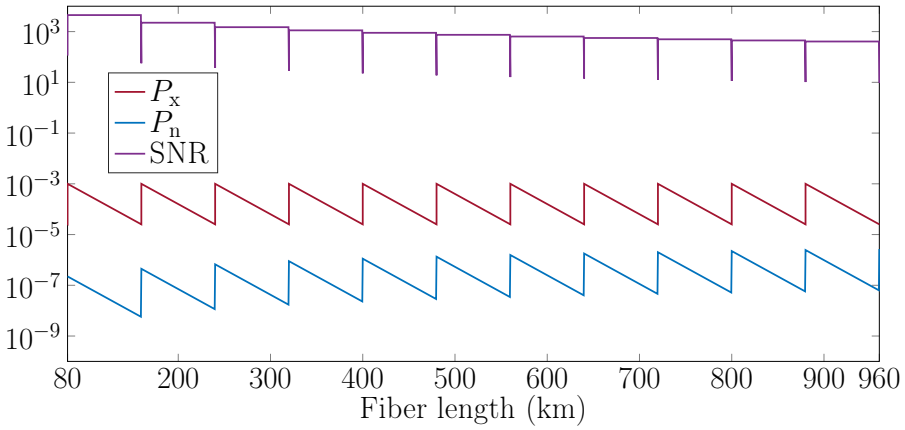

Figure 2.3: The power profile of the transmitted signal (P_x) signal with launched power of 10 dBm, ASE noise power (P_n), and the corresponding SNR over an SMF with length of 960 km.

Therefore, the propagated signal in the fiber experiences an exponential decay due to the fiber loss. Silica fibers exhibit wavelength-dependent fiber loss with minimum loss around 1550 nm, which corresponds to 0.2 dB/km. Thus, the center frequency of optical systems is usually set to 1550 nm. Due to the fiber loss, after a certain fiber length, it is required to amplify the signal in order to transmit over longer distances. The use of optical amplifiers in optical systems became widespread in the 1990s and by 1996 optical amplifiers were part of the fiber-optic cables laid across the Atlantic and Pacific oceans [53]. In order to compensate for the fiber loss, the optical fiber is divided into 80-120 km segments where each segment is equipped with an optical amplifier. Fig. 2.2 shows the schematic of a fiber optical system with N spans.

Optical amplifiers add noise to the amplified signal, i.e., the signal-to-noise ratio (SNR) of the signal is reduced by the amplifiers. There are two types of optical amplification. In the first type, known as *lumped amplification*, an amplifier boosts the received signal at the end of each span. The signal is amplified through stimulated emission, which introduces amplified spontaneous emission (ASE) noise. The power spectral density of the ASE noise per each polarization is given by $\mathrm{G_{ASE}}(\nu) = n_{\mathrm{sp}} h\nu\,(G-1)$, where n_{sp} is the spontaneous emission factor, $h\nu$ is the energy of a photon, and $G = \exp(\alpha L)$ is the gain of the amplifier for compensating the fiber loss in a span of length L. In the second type, known as *distributed amplification*, a pump signal transfers its energy to the original signal during prop-

agation through the so-called *stimulated Raman scattering* phenomenon, and the major source of amplifier noise is the spontaneous Raman scattering [55]. Fig. 2.3 shows the power profile of the input signal with launched power (P_x) of -10 dBm, the power of ASE noise due to lumped amplification (P_n), and the corresponding SNR in a system operating with 32 Gbaud data rate and amplifier noise figure of 4.5 dB, where the dispersion and nonlinearity are neglected, i.e., $\beta_2 = \gamma = 0$. As can be seen, by increasing the fiber length, the noise power gradually increases, i.e., the corresponding SNR reduces. Note that the power reduction is exponential over each span length, hence, it is linear in Fig. 2.3 with logarithmic scaling.

2.1.2 Kerr-Nonlinearity

The Kerr-nonlinearity is due to the fact that the refractive index of the fiber is power dependent. The second term in (2.2) represents the Kerr-nonlinearity effect. In the absence of dispersion, i.e., $\beta_2 = 0$, one can show that the Manakov equation has a closed-form solution given by

$$\boldsymbol{E}\left(t,z\right) = \boldsymbol{E}\left(t,0\right)\exp\left(-\alpha z/2\right)\exp\left(i\frac{8}{9}\gamma L_{\text{eff}}(z)||\boldsymbol{E}\left(t,0\right)||^2\right), \tag{2.4}$$

where $L_{\text{eff}}\left(z\right) = \frac{1-\exp(-\alpha z)}{\alpha}$ is called the effective length. As can be seen, the nonlinearity can be interpreted as a phase shift in the time-domain response which in turn leads to spectral broadening in the frequency domain, a phenomenon known as *self-phase modulation*. The nonlinear length, L_{NL}, is an important parameter and is defined as the fiber length after which the nonlinearity becomes important. For a pulse with peak power P_0 and nonlinear parameter γ, the nonlinear length is $L_{\text{NL}} = \frac{1}{\gamma P_0}$. As an example, $P_0 = -2$ dBm and $\gamma = 1.3$ (W.km)$^{-1}$ result in $L_{\text{NL}} = 485$ km.

2.1.3 Chromatic Dispersion

In fiber-optic communications, the group velocity is defined as the velocity of the signal envelope. Since the group velocity is frequency dependent, different components of the transmitted signal arrive at different times, which in turn leads to the time-domain broadening of the received signal. This phenomenon is known as GVD. To evaluate the effect of dispersion in the Manakov equation, one can neglect loss ($\alpha = 0$) and nonlinearity ($\gamma = 0$) and then find the solution for the Manakov equation as

$$\boldsymbol{E}\left(\omega,z\right) = \boldsymbol{E}\left(\omega,0\right)\exp\left(i\omega^2\frac{\beta_2}{2}z\right). \tag{2.5}$$

The GVD can also be expressed based on the dispersion parameter, defined as $D = -\frac{2\pi c\beta_2}{\lambda^2}$. In fact, the effect of GVD can be seen as a filter with frequency

response

$$\mathrm{H_{CD}}\left(\omega\right) = \exp\left(-i\frac{D\lambda^2 z}{4\pi c}\omega^2\right). \tag{2.6}$$

As can be seen, the dispersion behaves as an all-pass filter in the frequency domain with a phase with quadratic frequency dependency. The phase in the frequency domain results in pulse broadening in time domain, which in turn leads to inter-symbol interference. The dispersion length is defined as $L_D = \frac{1}{|\beta_2|\mathrm{W}^2}$, where W is the signal bandwidth. L_D indicates the approximate fiber length after which the dispersion becomes important, e.g., for $D = 17$ ps/nm/km and $\mathrm{W} = 32$ GHz, L_D=45 km.

CD can be compensated for in the optical domain, using dispersion compensating fibers [56], or in the digital domain, using DSP at the receiver [57]. In order to compensate the dispersion optically, each span is connected to a short length fiber, called dispersion compensating fiber, which has a dispersion parameter with the opposite sign compared to that of the underlying fiber. In coherent fiber-optic systems, the dispersion is compensated in the digital domain using DSP. According to (2.6), the frequency response of the CD compensation is an all-pass filter given as

$$\mathrm{H_{CD}^{-1}}\left(\omega\right) = \exp\left(i\frac{D\lambda^2 z}{4\pi c}\omega^2\right). \tag{2.7}$$

where c is the speed of light and λ is the wavelength. One approach to implement (2.7) is the frequency domain filtering using the overlap-save method [12]. In long-haul coherent optical communication, CD is usually compensated in the frequency domain since the number of time-domain filter taps becomes large and the complexity of implementation increases. On the contrary, we recently showed that it is beneficial from a complexity and energy consumption perspectives to use the time-domain CD compensation for short length links [12, 58].

Due to the importance of time-domain CD compensation in energy-efficient fiber optical systems, we elaborate a bit the main proposed structures in the literature [59–61]. To compensate the CD in time domain, one can design an FIR or IIR filters with the frequency response (2.7). Due to the inherent instability of IIR filters, FIR filters are of interest for CD compensation [59–61]. In [59], an FIR CD compensation filter, given in closed-form, was proposed by performing direct sampling (DS) and truncation of the ideal CD compensation impulse response.

The DS filter compensates the CD in the whole frequency band, while in a practical system the transmitted signal is band limited due to pulse shaping. Thus, the filter attempts to compensate the CD even in the frequency band without signal content. Therefore, potentially, one can reduce the number of filter taps and compensate the same accumulated CD by a better filter design. In [60], a new filter is proposed which takes into account the effect of pulse shaping at the transmitter. The proposed

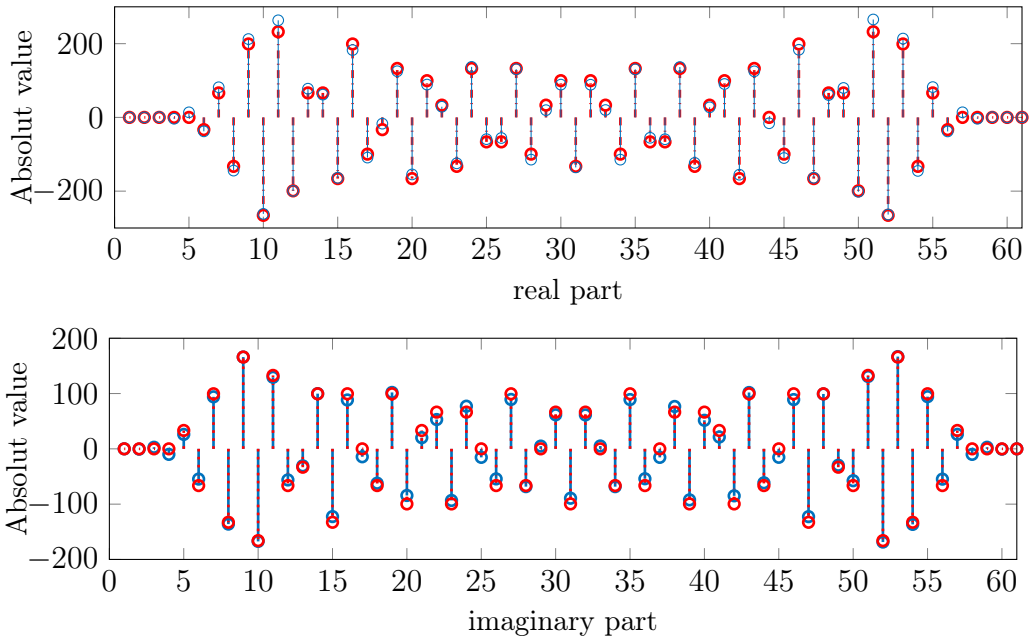

Figure 2.4: The real and imaginary parts of the filter coefficients of the LS-BL filter with 61 taps with floating point precision (blue) and quantized filter with 4-bit word length (red).

filter is based on a least-squares optimization problem given as

$$\tilde{\boldsymbol{h}} = \arg\min_{\boldsymbol{h}} \xi_s, \tag{2.8}$$

where $\boldsymbol{h} = [h_{-(N-1)/2}, \ldots, h_0, \ldots, h_{(N-1)/2}]^{\mathsf{T}}$ is the filter tap coefficient vector and ξ_s is the in-band error defined as the error between the frequency response of the ideal CD compensation filter and the frequency response of the FIR filter with coefficients $\boldsymbol{h}$ (see [60, Eg. 6]). For the ease of exposure, we refer to this filter as the least-squares band-limited (LS-BL) filter. As shown in [60], the LS-BL filter achieves the same performance as that of the DS filter with approximately 50% fewer number of filter taps. Since reducing the number of taps results in decreasing the implementation complexity and energy consumption accordingly, the LS-BL filter is a candidate for energy-efficient CD compensation. The works [59, 60] implicitly assume that filter taps are implemented with floating-point precision. In practice, however, filter taps must be implemented in finite precision. Coefficient quantization distorts the values of the coefficients, leading to quantization errors which, in turn, change the frequency response of the designed filter. As an example, consider the LS-BL filter with 61 taps, root-raised cosine pulse shaping and fiber parameters given in [61, Table I]. In Fig. 2.4, the real and imaginary parts of the filter tap coefficients of the LS-BL filter with floating point precision and the quantized filter using linear quantization [61, Sec. III.B] with 4-bit word length are shown. As can be seen, quantization alters the real and imaginary parts of the filter taps, which in turn changes both the amplitude and phase response of the underlying filter. Fig. 2.5 depicts the amplitude response of the

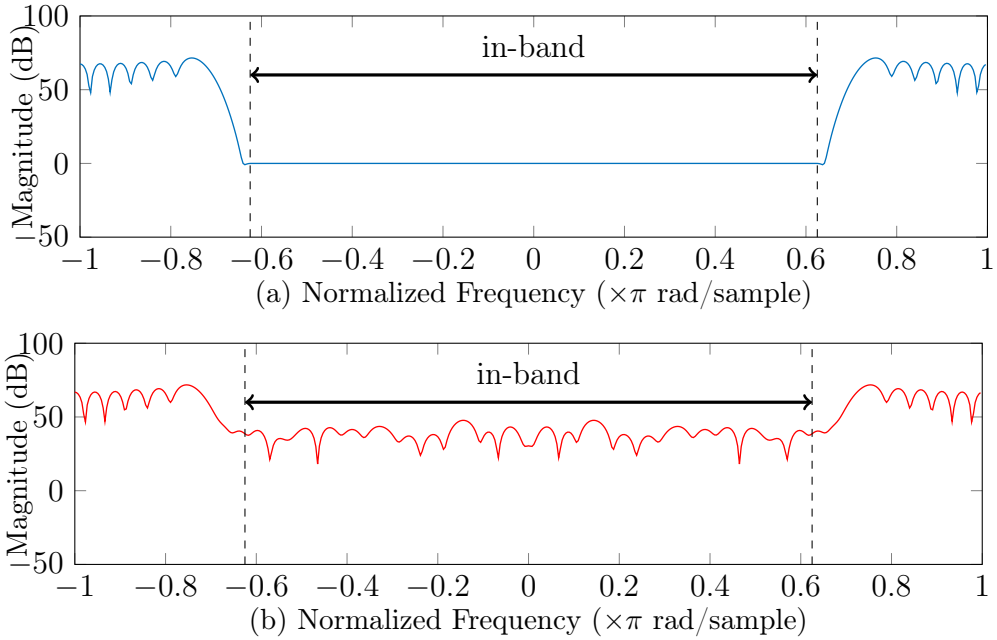

Figure 2.5: Amplitude response of the LS-BL filter with 61 taps and floating point precision (blue curve) and corresponding fixed-point filter using 4-bit word length (red curve).

LS-BL filter shown in Fig. 2.4. We remark that in Fig. 2.5 the in-band frequencies are $[-0.625\pi, 0.625\pi]$. It can be observed that the LS-BL filter with floating point precision provides the desired all-pass amplitude response while the in-band response of the quantized filter is significantly distorted. In fact, a high quantization error translates into a lot of distortion in the frequency domain. Therefore, it is required to incorporate the effect of quantization errors in the filter design, especially with respect to energy efficiency considerations, where the number of filter taps should be reduced as low as possible. In [61], we optimized the CD compensation filter taps using constrained least-squares method (LS-CO). Our proposed filter is given by

$$\tilde{\boldsymbol{h}} = \arg\min_{\boldsymbol{h}} \xi_s \tag{2.9}$$

$$\text{subject to} \quad \xi_o \leq \xi_{o,\max}, \tag{2.10}$$

where $\xi_{o,\max}$ is a selected threshold on the out-of-band gain. We have shown that by suppressing the out-of-band gain in (2.9), the resulting filter can be implemented with finite word length in DSP [58]. Deriving the LS-CO filter motivates recent studies on applying deep neural network for impairment compensation in fiber-optic systems [62].

2.1.4 Some other Impairments

Communication over the fiber-optic channel comes with some other impairments such as PMD and state-of-polarization (SOP) drifts. PMD results from the fact that the

light travels with different speeds for different polarizations, leading to differential group delay between two polarizations. In order to demultiplex the polarization-multiplexed signal, one needs to know the SOP, which may slowly drift with time in a random fashion. This phenomenon is known as the *SOP drift*. In this thesis we neglect these impairments, i.e., we assume that the SOP is perfectly tracked and that the light travels with the same speed for both polarizations.

2.2 Numerical Methods for Signal Propagation in Fiber-Optic Channels

Although the Manakov equation describes the signal propagation over the fiber-optic channel, as we have shown in Section 2.1, it only features a closed-form solution if the dispersion and/or Kerr-nonlinear effects are neglected. In general, there is no closed-form solution for solving (2.2), therefore one needs to numerically evaluate the signal propagation in the fiber-optic channel. The Split-step Fourier method [63] (SSFM) is mainly used to investigate the signal propagation along the fiber. In this section, we briefly describe the SSFM.

The Manakov equation (2.2) can be compactly written as

$$\frac{\partial \boldsymbol{E}(t,z)}{\partial z} = \tilde{L}\left(\boldsymbol{E}(t,z)\right) + \tilde{N}\left(\boldsymbol{E}(t,z)\right), \tag{2.11}$$

where $\tilde{L}(\cdot)$ and $\tilde{N}(\cdot)$ are operands representing the linear (dispersion and loss) an nonlinear (Kerr-nonlinearity) operations on the field envelop $\boldsymbol{E}(t,z)$. Although linear and nonlinear operations are acting jointly in signal propagation, for short distances, one can assume that $\tilde{L}(\cdot)$ and $\tilde{N}(\cdot)$ are independently applied to the input signal. In particular, in propagation from z to $z+\Delta$, one can neglect the linear effect ($\tilde{L}\left(\boldsymbol{E}(t,z)\right) = 0$) and just apply the nonlinear operand, i.e., the field envelop in time domain can be written as $\boldsymbol{E}(t,z+\Delta) = \boldsymbol{E}(t,z)\exp\left(j\frac{8}{9}\gamma\Delta||\boldsymbol{E}(t,z)||^2\right)$. The linear step can be implemented in the Fourier domain by neglecting the nonlinear step ($\tilde{N}\left(\boldsymbol{E}(t,z)\right) = 0$), i.e., the field envelop in frequency domain can be written as $\boldsymbol{E}(\omega,z+\Delta) = \boldsymbol{E}(\omega,z)\exp\left(i\omega^2\frac{\beta_2\Delta}{2}\right)\exp\left(-\frac{\alpha\Delta}{2}\right)$. Typically, the envelop is sampled and the operations are performed on samples. Note that the linear step can be efficiently implemented using the fast Fourier transform and the inverse the fast Fourier transform.

To propagate the signal over a fiber of length L, the fiber is divided into N different segments and each segment is divided into K different small sections of length Δ, i.e., $L = NK\Delta$. After applying the linear and nonlinear step for all samples K times, the signal is amplified and the corresponding ASE noise is added. Then, the same computation is done for all N segments in order to find the resulting signal at the receiver. In Fig. 2.6 the schematic of SSFM method is shown. The blue

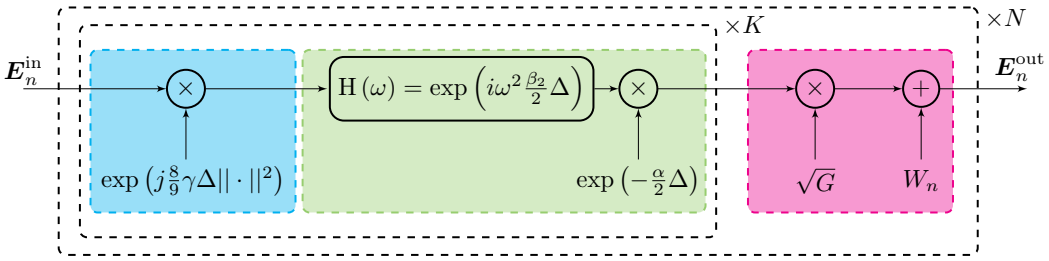

Figure 2.6: The schematic of SSFM method. $\boldsymbol{E}_n^{\text{in}}$ and $\boldsymbol{E}_n^{\text{out}}$ are vectors of input and output samples, respectively. The fiber length is L, which is divided to N segments and each segment is divided to K different steps. The blue, green, and red parts stand for linear, nonlinear, and amplification steps, respectively.

part represents the nonlinear step and the green one is the linear step. Furthermore, the red part represents the amplification step at the end of each span, where $G = \exp(\alpha\frac{L}{M})$, W_n is the ASE noise with variance $n_{\text{sp}}h\nu\left(G-1\right)/T_{\text{s}}$, T_{s} being the sampling rate.

2.2.1 Impairment Compensation in Fiber-Optic Channels

With the advent of coherent optical systems, impairment compensation is mainly performed at the receiver DSP. Here we briefly review two major categories of impairment compensation, namely electronic dispersion compensation (EDC) and digital back propagation (DBP), usually used as a benchmark to evaluate the system.

EDC compensates for the accumulated CD, i.e., Kerr-nonlinearity is neglected. To implement the EDC, the received signal is passed through a frequency domain or time domain filter (see Section 2.1.3), with accumulated dispersion corresponding to the fiber length.

DBP is a method to compensate for both linear and nonlinear impairments. DBP can be done at the transmitter as a pre-compensation [64,65] or at the receiver DSP as a post-compensation [57] or combination of both [66–69]. If one neglects the additive ASE noise, all impairments are deterministic. The idea of DBP is to back propagate the received signal digitally through a fiber with the same loss, nonlinear coefficient, and dispersion parameters as the original fiber but with opposite sign, i.e., $-\alpha$, $-\gamma$, and $-\beta_2$. DPB just compensates the so-called *signal-signal* interaction, and suffers from uncompensated *signal-noise* interaction. Stochastic DBP has been proposed to take also signal-noise interaction into account, but the corresponding complexity is rather high [70,71]. Recently, a DBP scheme based on deep neural networks has been proposed, showing promising gains with reasonable complexity [72]. To implement DBP, one can use the SSFM (See Fig. 2.6) excluding the noise, i.e., $W_n = 0$.

To give an impression on impairment compensation methods, we simulate the transmission of a single channel with symbol rate of 32 Gbaud, modulated with 16-

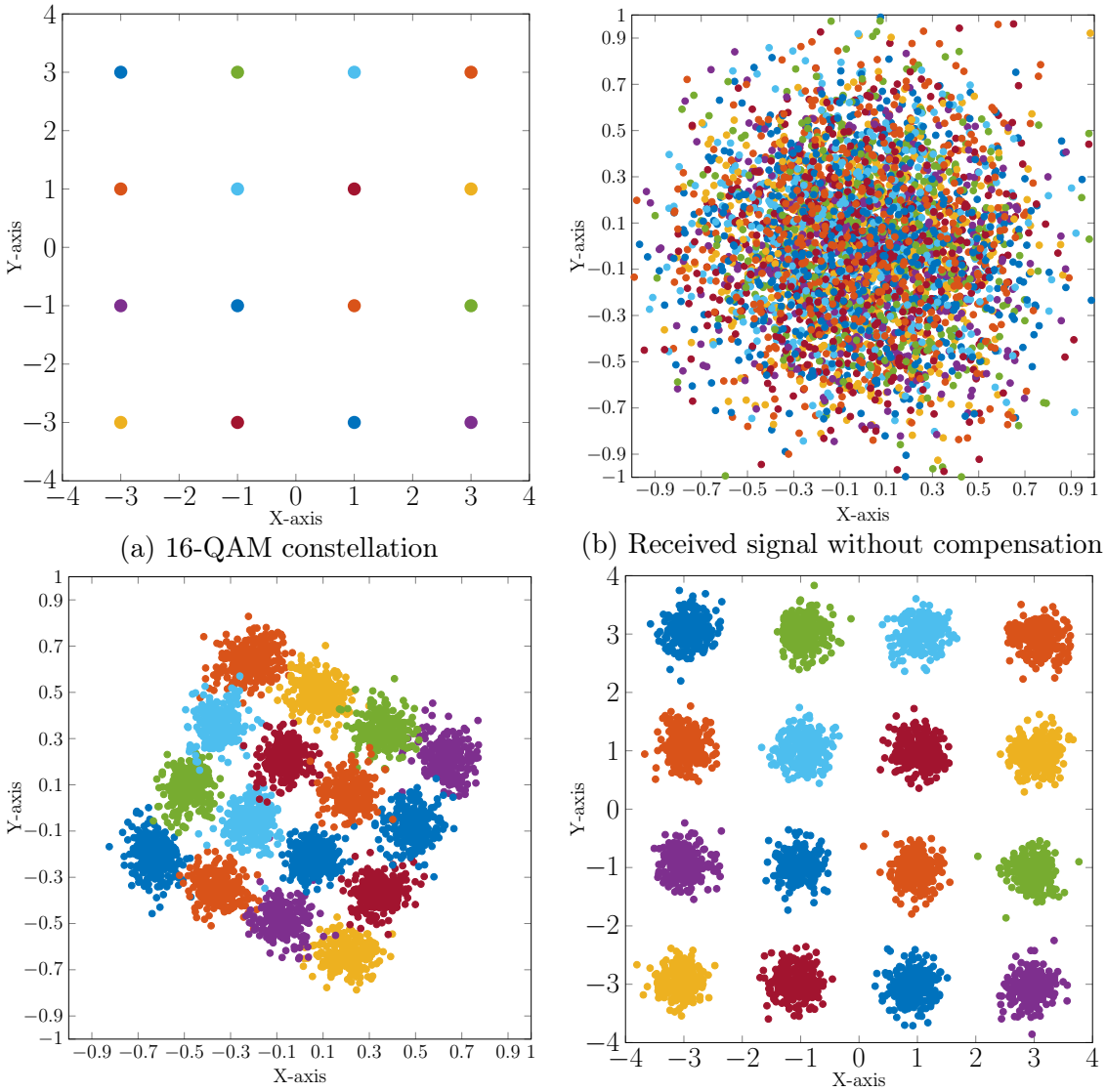

(a) 16-QAM constellation

(b) Received signal without compensation

(c) Compensated signal using EDC

(d) Compensated signal using DBP

Figure 2.7: Transmission simulation of 16-QAM modulation and corresponding compensations using DBP and EDC. 2^{12} symbols are transmitted using root raised cosine pulse shaping with roll-off factor 0.1 in SMF with length 960 km, $\alpha = 0.2$ dB/km, $D = 17$ ps/nm/km, $\gamma = 1.3$ (W.km)$^{-1}$, and amplifier noise figure of 4.5 dB.

QAM using root raised cosine pulse shaping with roll-off factor 0.1 over a 960 km SMF. Fig. 2.7 shows the received signal before performing compensation, as well as EDC and DBP compensations. As can be seen, the resulting constellation after EDC is rotated. This is due to uncompensated self-phase modulation. Note that there is a one-to-one mapping between each constellation point and the center of the received constellation clouds, hence, to perform maximum likelihood decision, one can consider the center of the constellation clouds as the transmitted constellation.

On the contrary, it can be seen that the self-phase modulation is compensated by DBP to a large extent. Furthermore, one can expect that the symbol error probability is largely improved by using DBP compared to EDC. This improvement is at the cost of the high complexity of DBP.

2.3 Gaussian Noise Channel Modeling

In order to design FEC for fiber-optic channels, one needs to first model the channel. As explained in Section. 2.2, a closed-form solution for (2.2) is unknown. Based on an study in 1993 [73], if the propagated signal has uncorrelated spectrum components, the nonlinear interference can be modeled as white noise. With the advent of coherent communication, the dispersion can be compensated for in the receiver DSP, making the assumption more realistic. Furthermore, several experimental results confirm that if the CD is left uncompensated in the optical link, the optical field has a Gaussian-like distribution [74–77]. This behavior is known as the Gaussian noise (GN) model [78–81]. More precisely, in the GN model, under certain conditions, it is shown that the interaction between nonlinearity and dispersion can be modeled accurately as a Gaussian distribution. The GN model is widely used in system design for point-to-point links as well as optical networks. For a wavelength-division multiplexing (WDM) system with J channels $j = 1, ..., J$ (J is assumed to be odd), each with center frequency f_j, bandwidth B_j, and power P_j, the nonlinear interference power spectral density (PSD) of channel j for each span and both polarizations is given as [81, Eq. (16)]

$$G_{\mathrm{sp}}^{\mathrm{NL}}(f_j) = \frac{3\gamma^2 G\left(f_j\right)}{2\pi\alpha\left|\beta_2\right|}\left[G^2\left(f_j\right)\ln\left|\frac{\pi^2\beta_2(B_j)^2}{\alpha}\right| + \sum_{\substack{j'=1\\ j'\neq j}}^{J} G^2\left(f_{j'}\right)\ln\left(\frac{|f_j - f_{j'}| + B_{j'}/2}{|f_j - f_{j'}| - B_{j'}/2}\right)\right], \tag{2.12}$$

where $G\left(f_j\right) = P_j/B_j$ is the signal PSD in channel j and f_j is the center frequency of the j-th channel. The received SNR for channel j is

$$\mathrm{SNR}_j = \frac{P_j}{N_{\mathrm{sp}}\left(G_{\mathrm{sp}}^{\mathrm{ED}}(f_j) + G_{\mathrm{sp}}^{\mathrm{NL}}(f_j)\right)B_j}, \tag{2.13}$$

where $N_{\mathrm{sp}} = L/L_{\mathrm{sp}}$, with L being the fiber length and L_{sp} the spanlength. We remark that with this model each WDM channel is modeled as an additive white Gaussian noise (AWGN) channel where the noise variance for channel j is $\sigma_j^2 = N_{\mathrm{sp}}\left(G_{\mathrm{sp}}^{\mathrm{ED}}(f_j) + G_{\mathrm{sp}}^{\mathrm{NL}}(f_j)\right)B_j$. Recently, it has been shown that the GN model can be modified to better match realistic scenarios, leading to the so-called enhanced GN model [82].

The validity of the GN model highly depends on the system parameters. In this thesis we target optical systems where the CD is compensated at the receiver.

Motivated by the GN model, we consider the AWGN channel to design our coding schemes. More precisely, in general we consider the memoryless complex-valued AWGN channel given as

$$y_{\mathrm{n}} = x_{\mathrm{n}} + z_{\mathrm{n}}, \tag{2.14}$$

where y_{n} is the channel output corresponding to input x_{n}, and z_{n} is the AWGN with variance $2\sigma^2$. Therefore, the conditional channel transition probability is given as

$$f_{Y_n|X_n}\left(y_n|x_n\right) = \frac{1}{2\pi\sigma^2}\exp\left(-\frac{|y_n - x_n|^2}{2\sigma^2}\right). \tag{2.15}$$

Chapter 3

Coded Modulation

In this chapter, we briefly introduce the CM concept as a method to increase the spectral efficiency. CM is particularly necessary for optical systems to cope with the ever increasing data rate demand. Essentially, in a CM system, FEC is combined with a higher order modulation in order to operate reliably at high spectral efficiencies. CM has been studied since the 1970s with different structures, depending on the code used (binary or nonbinary) and the way the code is combined with the higher-order constellation. In particular, trellis CM [83, 84], multi-level coding [85], CM with nonbinary codes [86], and bit-interleaved CM (BICM) [87] are major categories of CM schemes in the literature. In Papers A–C, we consider CM based on the BICM paradigm due to its inherently simple architecture. We also consider CM with nonbinary codes in Paper A and Paper B for comparisons.

3.1 Preliminaries

We assume a memoryless complex-valued AWGN channel as described in (2.14). The goal is to transmit data reliably in this channel. To operate at high spectral efficiencies, one should employ FEC in transmitting the data. More precisely, we define by $\mathcal{E}$ the encoder, which maps an information vector of dimension K to a codeword $\boldsymbol{c} \subset \{0, \cdots, s\}^N$ of dimension N. Furthermore, $\mathcal{D}$ is the decoder which maps a vector of length N to an information vector of dimension K. Notice that for $s = 1$, $\mathcal{E}$ and $\mathcal{D}$ are binary, while for larger values of s, they are referred to as nonbinary encoder and decoder, respectively. In order to send the encoded data over the AWGN channel, interfaces called mapper and modulator are required. The mapper usually assigns a label to the encoded data and the modulator usually maps each label to a complex value. In particular, QAM is primarily used in optical systems. The mapper is designed for a given modulation format in order to improve the performance of the overall CM system.

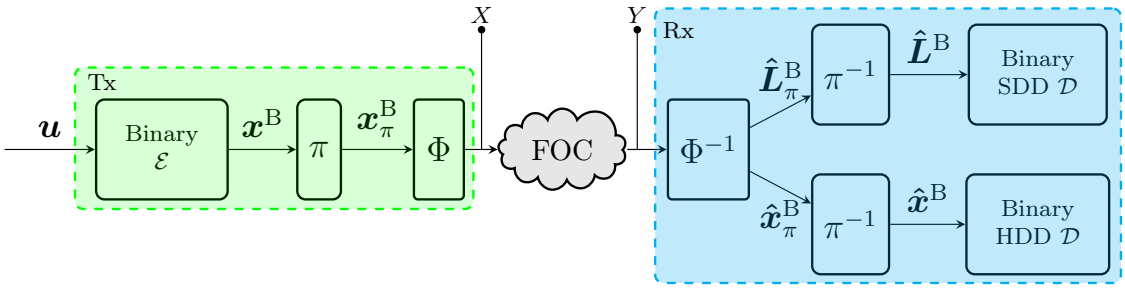

Figure 3.1: System model of the binary CM with SDD and HDD.

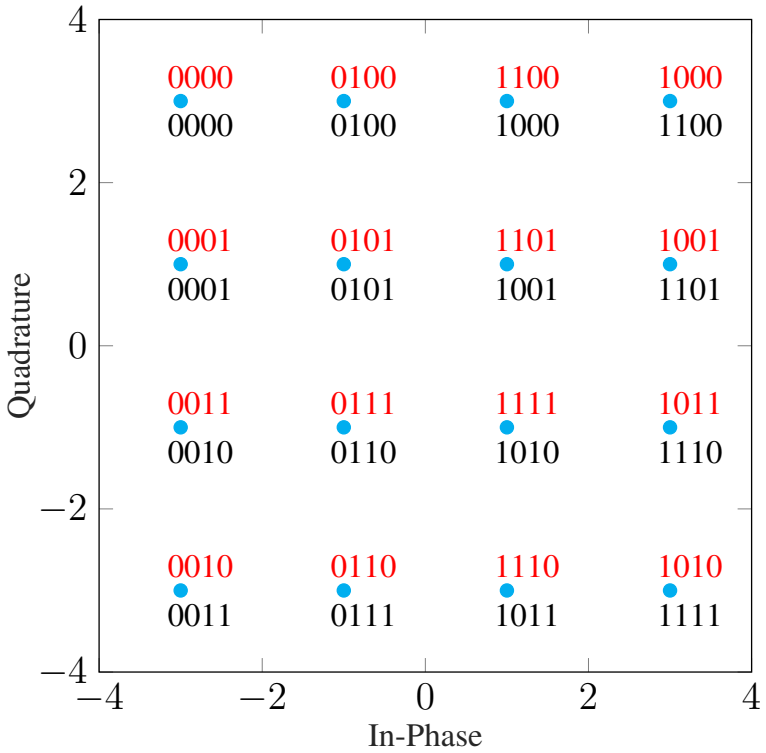

Figure 3.2: Gray (red) and natural (black) labeling of 16-QAM modulation.

3.2 Binary and nonbinary CM

Let us assume that $\mathcal{E}$ and $\mathcal{D}$ are binary, i.e., $s = 1$. Fig. 3.1 shows the system model of a binary CM system based on BICM. As can be seen, the binary information $\boldsymbol{u}$ is encoded by $\mathcal{E}$. The encoded data $\boldsymbol{x}^{\mathrm{B}}$ is then interleaved by an interleaver π, resulting in $\boldsymbol{x}_{\pi}^{\mathrm{B}}$. Then, $\boldsymbol{x}_{\pi}^{\mathrm{B}}$ is labeled by a mapper and modulated to constellation points. The sequence of modulated symbols is then transmitted over the fiber-optic channel (FOC). We remark that Φ in Fig. 3.1 stands for both mapping and modulation. In particular, for a QAM constellation of order 2^m, the mapper assigns groups of m bits to each constellation point. In Fig. 3.2, 16-QAM constellation with two different

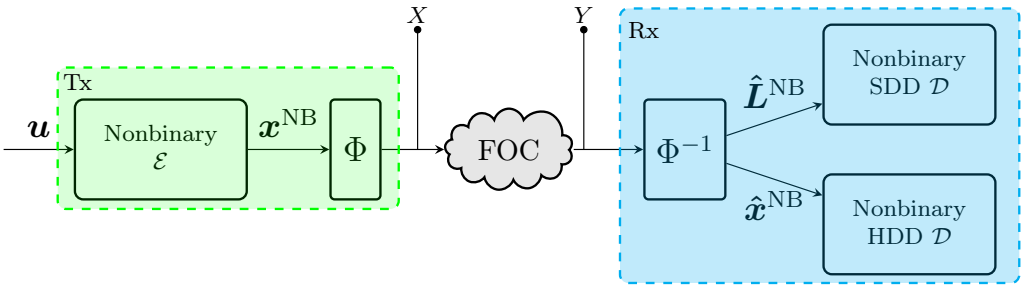

Figure 3.3: System model of the nonbinary CM with SDD and HDD decoders.

labelings, i.e., natural and Gray labeling are shown. For a given constellation point, the Gray labeling has the property that the binary representation of the neighboring constellation points differ only in one bit. This property reduces the number of bit errors at the input of the decoder, since most likely the noise changes the transmitted constellation point to one of the adjacent points. We remark that the role of the interleaver is to make the encoder and mapper independent.

The decoder can operate based on SDD or HDD. SDD exploits the channel reliabilities in the decoding, while HDD solely operates based on the Hamming distance metric [88–91]. As can be seen in Fig. 3.1, for SDD the demaper provides channel log-likelihoods, i.e., $\hat{\boldsymbol{L}}_{\pi}^{\mathrm{B}}$, and after de-interleaving passes $\hat{\boldsymbol{L}}^{\mathrm{B}}$ to the soft decision decoder. On the other hand, HDD provides a binary stream $\hat{\boldsymbol{x}}_{\pi}^{\mathrm{B}}$, resulting from hard detecting the channel observation, and after de-interleaving passes $\hat{\boldsymbol{x}}^{\mathrm{B}}$ to the decoder that operates based on the Hamming distance metric.

Fig. 3.3 shows the system model of a nonbinary CM system. The nonbinary message $\boldsymbol{u}$ is encoded to $\boldsymbol{x}^{\mathrm{NB}}$. We assume that the modulation order is matched to the construction field of the nonbinary code. Similar to its binary counterpart, at the decoder there are two possibilities, i.e., SDD or HDD. For SDD, the decoder computes likelihoods at the symbol level, then the resulting $\hat{\boldsymbol{L}}^{\mathrm{NB}}$ is sent to the nonbinary SDD decoder. For HDD, the demapper performs hard detection and $\boldsymbol{x}^{\mathrm{NB}}$ is sent to the nonbinary decoder based on HDD.

3.3 Achievable Information Rate for Coded Modulation

In order to evaluate the performance of CM systems, we need a performance metric. AIRs provide a lower bound on the mutual information, i.e., the maximum rate at which reliable transmission is possible, and are often used as the performance metric of CM systems. The memoryless assumption is commonly used in computing the AIRs of the FOC. With sufficiently long interleavering, this assumption is meaningful

for actual receivers. For computing the AIR of a CM system, a common approach is resorting to the mismatched decoding framework [92, 93]. The key idea behind mismatched decoding is to design a receiver that is optimum for an auxiliary channel (a good approximation of the true channel). We remark that the AIR is achievable with the optimal decoder for the auxiliary channel law.

Let us assume that at the receiver, for symbol-wise decoding, the received symbol y_i is hard detected to $\hat{x}_i$ using Φ^{-1} as

$$\hat{x}_i = \arg\max_{x \in \mathcal{X}} p_{Y|X}\left(y_i|x\right), \tag{3.1}$$

where $\mathcal{X}$ is the set containing the symbols of the constellation, of order M, and $\hat{\boldsymbol{x}}^{\mathrm{NB}} = (\hat{x}_1, \hat{x}_2, \ldots)$. For bit-wise decoding, we also consider that the received symbol y_i is hard detected according to (3.1). Then, $\hat{\boldsymbol{x}}^{\mathrm{B}}_{\pi} = (b(\hat{x}_1), b(\hat{x}_2), \ldots)$ is generated, where $b(\hat{x}_i)$ is a vector of m bits corresponding to the binary image of $\hat{x}_i$. After de-interleaving, $\hat{\boldsymbol{x}}^{\mathrm{B}}$ is available for bit-wise HDD (see Fig. 3.1). An achievable rate under the mismatched decoding metric q is given by the generalized mutual information (GMI) [92]

$$I^{\mathsf{gmi}} = \sup_{s>0} \mathbb{E}_{X,\hat{X}} \left[\log_2 \left(\frac{\mathrm{q}(\hat{X}, X)^s}{\frac{1}{M} \sum_{x \in \mathcal{X}} \mathrm{q}(\hat{X}, x)^s} \right) \right] \tag{3.2}$$

where X and $\hat{X}$ are RVs corresponding to the transmitted and hard–detected symbols (see Fig. 3.1 and Fig. 3.3), $\mathbb{E}(\cdot)$ is the expectation with respect to the joint distribution $p(\hat{X}, X)$ of the FOC, M is the order of the constellation set $\mathcal{X}$, $\mathrm{q}(\hat{X}, X)$ is a decoding metric corresponding to the auxiliary memoryless channel, and s is an optimization parameter.

In [94], the AIR of both binary and nonbinaty CM was computed, assuming that the decoder is assisted with the channel transition probabilities resulting from performing hard detection by Φ^{-1}. It is shown that for such a decoder, nonbinary codes achieves higher AIRs than their binary counterparts. We remark that this decoder can not be necessarily implemented with low complexity, since the soft information due to hard detection should be also exploited in the decoding. As explained in Chapter 1, we are interested in a HDD system that operates solely based on the Hamming distance metric, which can be implemented with low complexity using the Berlekamp-Massey algorithm [51, 95]. Therefore, in paper A we derive the AIR for both binary and nonbinary CM with HDD based on the mismatched decoding approach. Contrary to [94], we show that binary codes achieve higher AIR compared to their nonbinary counterpart. In Paper A, the AIR derivation for nonbinary HDD CM is provided, while for the binary case, the sketch of the proof is explained. In the following, we provide a complete proof for the AIR of the bit-wise HDD.

3.3.1 Achievable Information Rate of bit-wise Hard Decision Decoding

As explained before, for HDD one should consider the Hamming distance metric. It is easy to observe that employing the Hamming distance metric is equivalent to maximizing the mismatched metric

$$\mathrm{q}(b_i(\hat{x}), b_i(x)) = \begin{cases} 1-\hat{\epsilon} & \text{if } b_i(\hat{x}) = b_i(x) \\ \hat{\epsilon} & \text{otherwise} \end{cases}, \tag{3.3}$$

where ϵ is an arbitrary value in $(0, 1/2)$ and $b_i(x)$ is the ith bit of the label $b(x)$. Let us assume that a binary codeword $\boldsymbol{x}$ with length N corresponds to the binary image of N' symbols, each with $m = \log_2(M)$ bits, i.e., $\boldsymbol{x} = (b(x_1), \cdots, b(x_{N'}))$. It is easy to verify that the decoded codeword $\hat{\boldsymbol{x}}_{\mathsf{HDD-BW}} = (b(\hat{x}_1), \cdots, b(\hat{x}_{N'}))$ under optimal decoding with metric (3.3) is given as

$$\begin{aligned} \hat{\boldsymbol{x}}_{\mathsf{HDD-BW}} &= \arg\max_{\boldsymbol{x}\in\mathcal{C}} \prod_{i=1}^{N'} \prod_{j=1}^{m} \mathrm{q}(b_j(\hat{x}_i), b_j(x_i)) \\ &= \arg\max_{\boldsymbol{x}\in\mathcal{C}} \prod_{i=1}^{N'} \hat{\epsilon}^{d_{\mathrm{H}}(b(\hat{x}_i), b(x_i))} (1-\hat{\epsilon})^{m - d_{\mathrm{H}}(b(\hat{x}_i), b(x_i))} \\ &= \arg\max_{\boldsymbol{x}\in\mathcal{C}} \epsilon^{\sum_{i=1}^{N'} d_{\mathrm{H}}(b(\hat{x}_i), b(x_i))} \\ &\overset{(a)}{=} \arg\min_{\boldsymbol{x}\in\mathcal{C}} \sum_{i=1}^{N'} d_{\mathrm{H}}\left(b(\hat{x}_i), b(x_i)\right), \end{aligned} \tag{3.4}$$

where (a) holds if and only if $0 < \epsilon < 1$. From (3.4), we can see that for the bit-wise decoding with Hamming distance metric, the mismatched metric between the RV of transmit symbol X and the hard detected symbol $\hat{X}$ is

$$q(X, \hat{X}) = \epsilon^{d_{\mathrm{H}}\left(b(\hat{X}), b(X)\right)}. \tag{3.5}$$

Substituting (3.5) in (3.2), we have

$$I^{\mathsf{gmi}}_{\mathsf{HDD-BW}}(X; \hat{X}) = m + \sup_{s>0} \mathbb{E}_{X,\hat{X}} \left[\log_2 \frac{\epsilon^{s d_{\mathrm{H}}\left(b(\hat{X}), b(X)\right)}}{\sum\limits_{\mathbf{a}\in\{0,1\}^m} \epsilon^{s d_{\mathrm{H}}\left(b(\hat{X}), b(\mathbf{a})\right)}} \right], \tag{3.6}$$

which can be written as

$$I^{\mathsf{gmi}}_{\mathsf{HDD-BW}}(X; \hat{X}) = m + \sup_{s>0} \mathbb{E}_{X,\hat{X}} \left[\log_2 \frac{\epsilon^{s \sum\limits_{i=1}^{m} \mathbb{1}_{\mathrm{H}}\left(b_i(\hat{X}), b_i(X)\right)}}{\sum\limits_{\mathbf{a}\in\{0,1\}^m} \epsilon^{s \sum\limits_{i=1}^{m} \mathbb{1}_{\mathrm{H}}\left(b_i(\hat{X}), b_i(\mathbf{a})\right)}} \right], \tag{3.7}$$

where

$$\mathbb{1}_{\mathrm{H}}\left(b_i(\hat{x}), b_i(x)\right) = \begin{cases} 1 & \text{if } b_i(\hat{x}) = b_i(x) \\ 0 & \text{if } b_i(\hat{x}) \neq b_i(x) \end{cases}. \tag{3.8}$$

Then we have

$$I^{\mathsf{gmi}}_{\mathsf{HDD-BW}}(X;\hat{X}) = m + \sup_{s>0} \mathbb{E}_{X,\hat{X}} \left[\log_2 \frac{\prod_{i=1}^{m} \epsilon^{s\mathbb{1}_{\mathrm{H}}\left(b_i(\hat{X}), b_i(X)\right)}}{\prod_{i=1}^{m} \sum_{a\in\{0,1\}} \epsilon^{s\mathbb{1}_{\mathrm{H}}\left(b_i(\hat{X}), b(a)\right)}} \right], \tag{3.9}$$

which is simplified as

$$I^{\mathsf{gmi}}_{\mathsf{HDD-BW}}(X;\hat{X}) = m + \sup_{s>0} \sum_{i=1}^{m} \mathbb{E}_{X,\hat{X}} \left[\log_2 \frac{\epsilon^{s\mathbb{1}_{\mathrm{H}}\left(b_i(\hat{X}), b_i(X)\right)}}{\sum_{a\in\{0,1\}} \epsilon^{s\mathbb{1}_{\mathrm{H}}\left(b_i(\hat{X}), b(a)\right)}} \right], \tag{3.10}$$

One can easily show that (3.10) corresponds to

$$I^{\mathsf{gmi}}_{\mathsf{HDD-BW}}(X;\hat{X}) = m + m \sup_{s>0} \mathbb{E}_{X_{\mathrm{U}},\hat{X}_{\mathrm{U}}} \left[\log_2 \frac{\epsilon^{s\mathbb{1}_{\mathrm{H}}\left(b(X_{\mathrm{U}}), b(\hat{X}_{\mathrm{U}})\right)}}{\sum_{a\in\{0,1\}} \epsilon^{s\mathbb{1}_{\mathrm{H}}\left(b(\hat{X}_{\mathrm{U}}), b(a)\right)}} \right], \tag{3.11}$$

where X_{U} and $\hat{X}_{\mathrm{U}}$ are the RVs representing uniformly distributed bit positions over the binary representation of the transmitted symbol and hard detected symbol, respectively. Therefore, we have

$$\begin{aligned} I^{\mathsf{gmi}}_{\mathsf{HDD-BW}}(X;\hat{X}) =& m + m \sup_{s>0} \log_2 \frac{\epsilon^s}{1+\epsilon^s} . p\left(b(\hat{X}_{\mathrm{U}}) = b(X_{\mathrm{U}})\right) && (3.12) \\ &+ \log_2 \frac{1}{1+\epsilon^s} . p\left(b(\hat{X}_{\mathrm{U}}) \neq b(X_{\mathrm{U}})\right), && (3.13) \end{aligned}$$

We define the RVs E and F as follows,

$$E = \begin{cases} 1 & \text{if } \dfrac{\epsilon^s}{1+\epsilon^s} \\ 0 & \text{if } \dfrac{1}{1+\epsilon^s} \end{cases} \tag{3.14}$$

$$F = \begin{cases} 1 & \text{if } p\left(b(\hat{X}_{\mathrm{U}}) = b(X_{\mathrm{U}})\right) \\ 0 & \text{if } p\left(b(\hat{X}_{\mathrm{U}}) \neq b(X_{\mathrm{U}})\right) \end{cases}, \tag{3.15}$$

The Kullback–Leibler divergence between two RVs is a positive value, i.e., $\mathbb{D}(F||E) > 0$ [96], hence, one can easily show that

$$\mathbb{E}_F(\log_2 E) \leq \mathbb{E}_F(\log_2 F) \tag{3.16}$$

where $\mathbb{E}_F(\log_2 F) = -h_\mathrm{b}(F)$ and $h_\mathrm{b}(\cdot)$ is the binary entropy function. From the definition of $\hat{X}_\mathrm{U}$ and X_U, one can infer that $p\left(b(\hat{X}_\mathrm{U}) \neq b(X_\mathrm{U})\right)$ is the average probability of error over the bit positions of the binary representation of the symbols $\hat{X}$ and X. In other words, if we define ϵ_i as the crossover probability of the i-th bit level, then $\bar{\epsilon} = \frac{1}{m}\sum_{i=1}^{m} \epsilon_i = p\left(b(\hat{X}_\mathrm{U}) \neq b(X_\mathrm{U})\right)$. From (3.12) and (3.16), one can conclude that

$$I^{\mathsf{gmi}}_{\mathsf{HDD-BW}}(X;\hat{X}) \leq \sup_{s>0} m - m h_\mathrm{b}(\bar{\epsilon}). \tag{3.17}$$

According to (3.15), (3.14), and (3.16), the equality happens when E and F have the same distribution. Selecting s such that $\bar{\epsilon} = \frac{1}{1+\epsilon^s}$ yields

$$I^{\mathsf{gmi}}_{\mathsf{HDD-BW}}(X;\hat{X}) = m - m h_\mathrm{b}(\bar{\epsilon}). \tag{3.18}$$

As can be seen, by defining a proper decoding metric in the mismatched decoding framework, $I^{\mathsf{gmi}}_{\mathsf{HDD-BW}}(X;\hat{X})$ is computed. Equation (3.18) has a clear interpretation: in a BICM system with Hamming distance metric, all bit channels are treated equally, irrespective of their channel quality, hence from the decoder perspective the CM scheme is seen as m parallel binary symmetric channels each with crossover probability $\bar{\epsilon}$. We remark that if the decoder is assisted with information about the channel transition probabilities of the m bit channels, one can achieve a higher AIR than (3.18). We refer to this case as hard detector/channel-aware decoder (HdChaD) in Paper A. The AIR of bit-wise HdCha is given as [94]

$$I^{\mathsf{gmi}}_{\mathsf{HdChaD-BW}} = m - \sum_{i=1}^{m} h_\mathrm{b}(\epsilon_i). \tag{3.19}$$

In Fig. 3.4 we compare the AIR for 16-QAM, 64-QAM, and 256-QAM modulations. As can be seen, $I^{\mathsf{gmi}}_{\mathsf{HdChaD-BW}}$ is larger than $I^{\mathsf{gmi}}_{\mathsf{HDD-BW}}$ for all modulation formats. We remark that the AIR improvement of $I^{\mathsf{gmi}}_{\mathsf{HdChaD-BW}}$ is at the cost of significant implementation complexity compared to HDD.

3.4 Hard Decision Forward Error Correction

SDD based on LDPC codes has been adopted in fiber-optic systems due to providing large net coding gains. This excellent net coding gain comes at the cost of high decoding data flow and decoder energy consumption. To reduce the decoding data

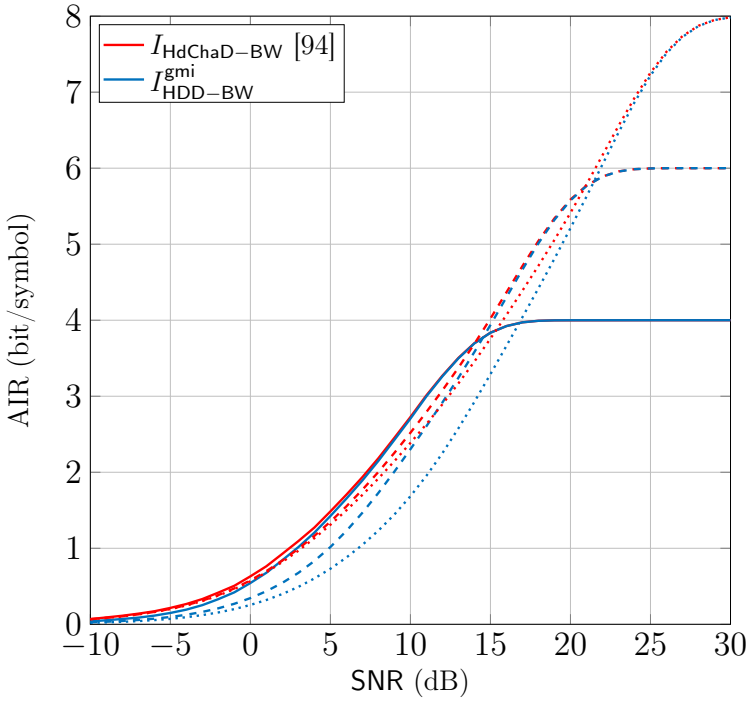

Figure 3.4: AIRs of the bit-wise CM with 16-QAM (solid), 64-QAM (dashed), and 256-QAM (dotted) modulations for HDD and HdChaD.

flow, hard decision FEC (HD FEC) is an appealing alternative [29, 39, 97]. HD FEC has been used historically in optical systems. In particular, BCH and RS codes are used as binary and nonbinary FEC codes in many optical experiments.

BCH codes are a class of cyclic codes invented by Hocquenghem [83] and Bose and Chaudhuri [98] independently around 60 years ago. For an $(n,k,d_{\min})$ BCH code with length n, dimension k, and minimum Hamming distance $d_{\min}$, the following conditions hold

$$n = 2^{\nu} - 1, \quad n - k \leq \nu t, \quad d_{\min} \geq 2t + 1, \tag{3.20}$$

where the Galois field GF(2^{ν}) is the construction field of the BCH code and t is the error correction capability of the code. In order to provide different code rates, one can build an expurgated code by simply shortening a BCH code. Shortening means that some of the information positions are deliberately substituted with zeros, where these bits are known at the decoder. A shortened BCH code with $(\tilde{n}, \tilde{k}, \tilde{d}_{\min})$ is given as

$$\tilde{n} = 2^{\nu} - 1 - s, \quad \tilde{k} = k - s, \quad \tilde{d}_{\min} \geq d_{\min}, \tag{3.21}$$

where s is the number of shortened bits.

RS codes are a generalization of BCH codes for the nonbinary case and invented by Reed and Solomon in 1960 [99]. The symbols of a RS code are from the Galois field GF(2^{ν}) and each symbol can be represented with ν bits. An $(n, k, d_{\min})$ RS code

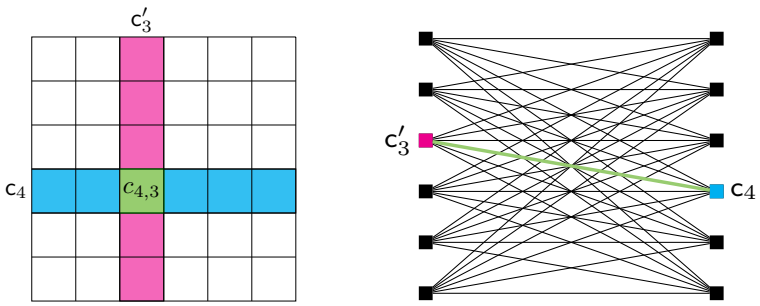

Figure 3.5: Code array (left) and simplified Tanner graph (right) for a PC with a component code of length $n = 6$. In the simplified Tanner graph, degree-2 VNs are omitted and instead represented as simple edges.

has parameters

$$n = 2^{\nu} - 1, \quad n - k = 2t, \quad d_{\min} = 2t + 1. \tag{3.22}$$

Similar to BCH codes, one can generate expurgated RS codes by shortening. The relation between the shortened RS code $(\tilde{n}, \tilde{k}, \tilde{d}_{\min})$ and the original RS code $(n, k, d_{\min})$ is given as

$$\tilde{n} = n - s, \quad \tilde{k} = k - s, \quad \tilde{d}_{\min} = d_{\min}. \tag{3.23}$$

In order to achieve high net coding gains for HDD, powerful code constructions such as PCs, half PCs [37], braided codes [38], and staircase codes [29], and other generalized PCs [39] build over component BCH/RS codes have been proposed. In this thesis, we particularly consider PCs and staircase codes due to their excellent performance-complexity trade-offs. In the following, we briefly review PCs and staircase codes.

3.4.1 Product Codes

PCs were introduced by Elias in 1954 [36] as a method for generating a powerful code with large blocklength based on a short–length component codes. The iterative decoding of PCs dates back to 1968 [100], while it regained attention after employing SDD based on the turbo principle, which improved the coding gain extensively [18]. PCs also provide a good coding gain with low-complex iterative BDD of the underlying component codes. Let $\mathcal{C}$ be a BCH code with parameters $(n, k, d_{\min})$. A binary (two-dimensional) PC with parameters $(n^2, k^2, d_{\min}^2)$ and rate $R = k^2/n^2$ is defined as the set of all $n \times n$ rectangular arrays such that each row and column of the array is a codeword of $\mathcal{C}$. Correspondingly, a codeword of the PC can be represented as a binary matrix $\boldsymbol{C} = [c_{i,j}]$ of size $n \times n$. Alternatively, a PC can be defined via a Tanner graph with $2n$ constraint nodes (CNs), where n CNs correspond to the row codes and n CNs correspond to the column codes. The graph has n^2 variable nodes (VNs) corresponding to the n^2 code bits. The code array and (simplified) Tanner

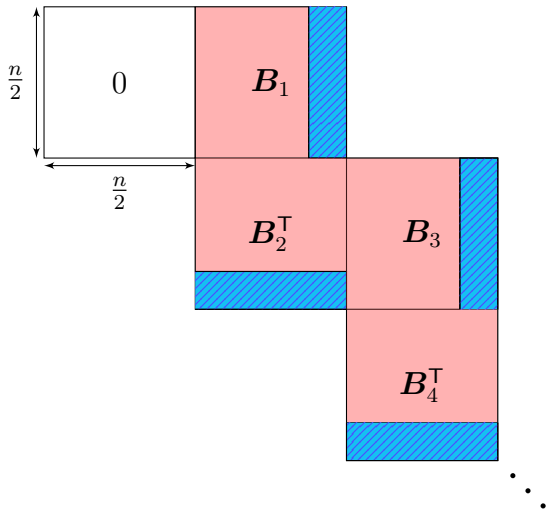

Figure 3.6: The code array of a staircase code. Information bits and parity bits are shown with red color and blue hatches, respectively.

graph of a PC with $n = 6$ is shown in Fig. 3.5. In Papers D-F PCs are employed in the proposed schemes.

3.4.2 Staircase Codes

Binary staircase codes with BCH component codes, proposed by Smith *et al.* [29], provide large net coding gains. The staircase code in [29] with roughly 7% OH provides 0.42 dB net coding gain improvement compared to the best proposed code from the ITU-T G.975.1 recommendation at a bit error rate of 10^{-15}. The impressive performance of staircase codes, together with their low–complexity algebraic decoding, makes them an interesting option for future fiber-optic systems.

A staircase codes is defined by a two-dimensional array, which is shown in Fig. 3.6. Similar to PCs, the structure of the staircase code imposes that each code bit is protected by two component codes, a row code and a column code. For the encoding, the first block of the code array is initialized with zeros. Information bits are then placed in the first part of the second block (shown with red color in Fig. 3.6), and represented by a binary matrix $\boldsymbol{B}_1$. By row encoding, parity bits (shown with blue hatches) are generated. Then, data bits are placed in the first part of the third block, represented by a binary matrix $\boldsymbol{B}_2$ (see Fig. 3.6), and column encoding is performed. This procedure continues for encoding the next blocks. In particular, each row of $[\boldsymbol{B}_{\text{i-1}}^{\mathsf{T}}, \boldsymbol{B}_{\text{i}}]$ is a valid codeword of the BCH component code. In Papers A-D, we consider staircase codes in our proposed schemes.

In order to design the component codes of PCs and staircase codes, a straightforward approach is resorting to Monte-Carlo simulations, as considered in [40]. To make the code parameter optimization faster, one can evaluate the performance of

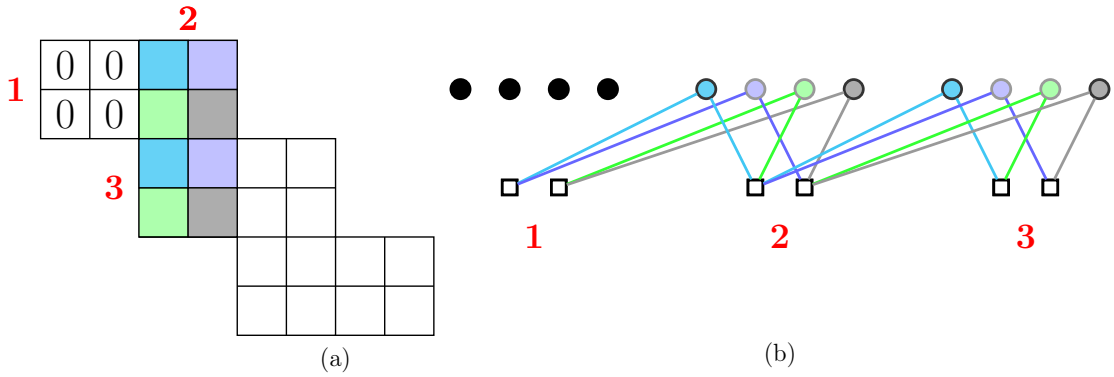

Figure 3.7: (a) An example of a staircase code with 4 coded symbols per each spatial position, and (b) the corresponding bipartite graph.

the code ensemble corresponding to PCs and staircase codes using a mathematical tool called DE [39]. In the following, we briefly explain the idea behind DE.

3.4.3 Density Evolution

DE is a mathematical tool to estimate the asymptotic performance of codes-on-graphs. More precisely, the DE allows to predict the iterative decoding threshold of a code ensemble, i.e., the worst channel parameter for which the probability of error goes to zero under belief propagation decoding (as the block length goes to infinity). In coding theory, determining the iterative decoding threshold for a particular (deterministic) code is very difficult. In contrast, analyzing code ensembles is much easier. One can use the DE analysis to optimize code parameters so that the iterative decoding threshold is optimized.

PCs are contained in the ensemble of generalized LDPC (GLDPC) codes. From Fig. 3.5, we can observe that the bipartite graph of a PC is similar to that of an LDPC code with the difference that CNs are BCH codes rather than single parity-check codes. Furthermore, staircase codes can be seen as a class of SC-GLDPC codes [41]. In Fig. 3.7(a), we depict the code array of a staircase code with 4 code symbols per block and the corresponding bipartite graph. In the bipartite graph, each staircase block corresponds to one spatial position. As an example, the first three blocks and spatial positions are numbered in Fig. 3.7. In the bipartite graph, the VNs, represented by circles, correspond to code symbols, while the CNs, represented by squares, correspond to the row and column codes. For instance, the squares in spatial position 1 correspond to the first two row codes while the squares in spatial position 2 correspond to the first two column codes. An edge is drawn between a VN and a CN if the corresponding code bit participates in the corresponding row/column code. In the figure, the code symbols and the corresponding edges for spatial positions 2 and 3 are shown with the same color, e.g., in Fig. 3.7(b), the first code symbol in spatial position 2 (shown in blue), is connected to the first component code in

spatial positions 1 and 2. As can be seen, each code symbol in spatial position i is connected to one component code in spatial position i and one component code in spatial position $i-1$. From Fig. 3.7, one can readily infer that the staircase code is contained in the ensemble of SC-GLDPC codes with coupling width 2 [41].

In the DE analysis, the densities of the messages exchanged in the iterative decoding are tracked over decoding iterations. In particular for HDD of product-like codes, error probability of the messages at the output of the CNs is tracked over decoding iterations. In [101], the DE for HDD and binary SC-GLDPC codes with BCH component codes was derived. In [41], the parameters of staircase codes were optimized using the DE derived in [101] to optimize the iterative decoding threshold. In Papers A-B, we extend the DE analysis in [101] to HDD of nonbinary SC-GLDPC codes with RS component codes. Then, we use the derived DE to design the parameters of nonbinary staircase codes with RS component codes. The optimized nonbinary staircase codes are used to verify the AIR analysis in Paper A. Furthermore, in Paper D we derive a DE for both GLDPC and SC-GLDPC ensembles under iBDD-SR in order to optimize the design parameter of the proposed algorithm for both PCs and staircase codes.

Chapter 4

Performance Improvement Techniques

CM with equally-spaced constellation points and uniform signaling provides high spectral efficiencies, but still there is a gap to the channel capacity. This gap is mainly due to two reasons. First, the decoding method is usually suboptimal in order to reduce the decoder complexity. Second, the uniform signaling is not capacity-achieving. Therefore, there is a research line in improving the performance of CM systems using different kinds of signal shaping and different decoding architectures. In this chapter, we briefly explain the concept of signal shaping, then we explain the state-of-the-art decoding architectures for HDD. The content of this chapter is mainly related to Papers C-F.

4.1 Signal Shaping

For the AWGN channel, it is well-known that the capacity-achieving distribution is Gaussian. Therefore, conventional QAM constellations with uniform signaling will experience a performance loss over the AWGN channel. In the asymptotic regime where the SNR and the order of the constellation are large, this gap is 1.53 dB. Signal shaping is a method to shape the constellation points in order to mimic the capacity-achieving distributions, yielding a smaller gap to capacity.

There are two main classes of signal shaping, namely, geometric shaping [42–46] and probabilistic shaping [47–49]. In geometric shaping, non equidistant constellation points are employed such that the overall constellation mimics the capacity-achieving distribution. The best constellation depends on the received SNR and also the employed decoding metric. Although geometric shaping has been used in fiber-optic systems [46, 102–104], it is less popular compared to probabilistic shaping due to some practical issues. In particular, since the optimal geometrically-shaped constellation differs for different SNRs, in principle it is required to have a large resolution of the analog-to-digital converter in order to capture the received signal. Furthermore, [105] shows that geometric shaping suffers from a 0.4 dB performance

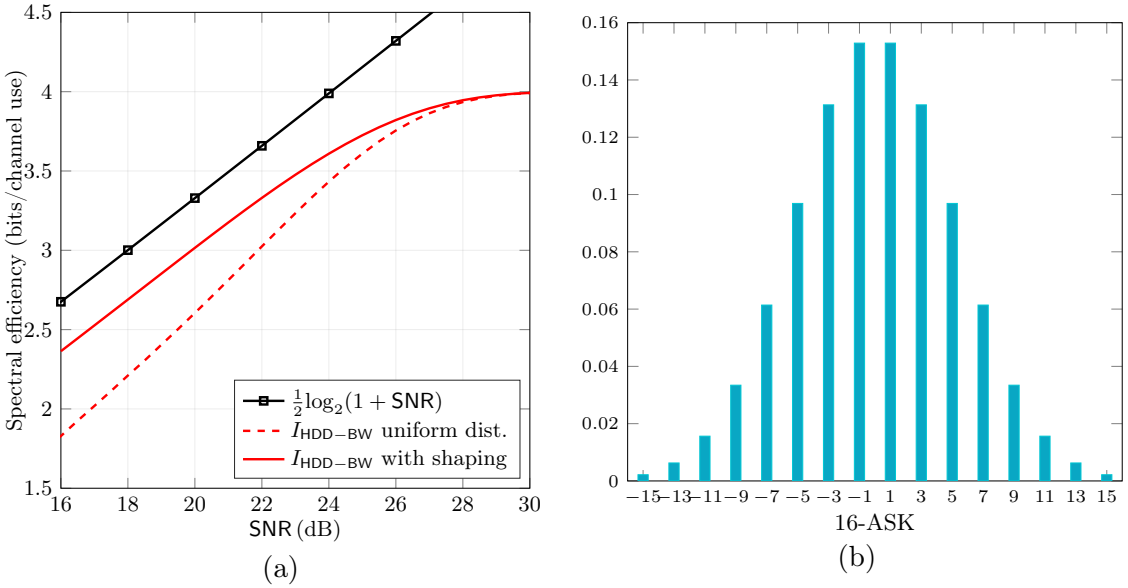

(a) (b)

Figure 4.1: (a) The AIR of bit-wise HDD for 16-ASK with uniform and probabilistic shaping. (b) The optimized distribution of 16-ASK, corresponding to $\mathsf{SNR} = 20$ dB.

degradation compared to probabilistic shaping when bit-wise decoding is employed.

Probabilistic shaping uses a conventional constellation with equidistant constellation points and nonuniform signaling to mimic the capacity-achieving distribution. The advantage of probabilistic shaping is that it uses off-the-shell constellations, which is desirable from an implementation perspective. In Fig. 4.1(a), the AIRs of 16-ASK with uniform and probabilistically-shaped distribution are shown for bit-wise HDD. For the sake of illustration, we also show the optimized distribution for 16-ASK with $\mathsf{SNR} = 20$ dB in Fig. 4.1(b). As can be seen, the AIR of the shaped constellation is much larger than the AIR with uniform signaling. Furthermore, the optimal distribution resembles the Gaussian distribution.

4.1.1 Probabilistic Amplitude Shaping

From Fig. 4.1(b), one can see that the optimal distribution is symmetric, as expected due to the symmetry of the AWGN channel. Therefore, it is only required to shape the amplitudes of the constellation points and then use a uniform sign to obtain the fully-shaped constellation. This observation motivates the scheme known as PAS, which has been recently proposed by Böcherer *et al.* [49] and gained lots of attention in the optical community [106–112]. The key idea of PAS is to move the shaping of the amplitudes before the encoding, contrary to conventional probabilistic shaping, and use the (uniformly distributed) parity bits at the output of a systematic encoder along with some information bits to generate the uniform signs. The system model of PAS is shown in Fig. 4.2. For the ease of explanation, we consider PAS with an underlying

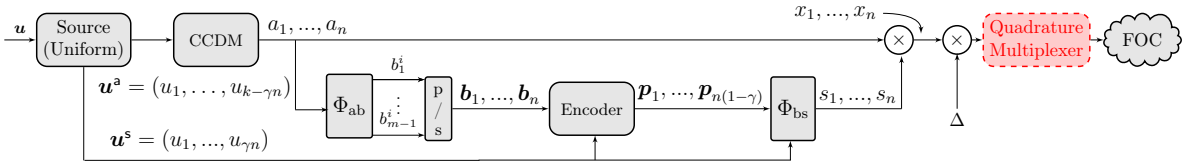

Figure 4.2: Block diagram of the PAS scheme.

ASK constellation, i.e, the constellation points are chosen from the set $\mathcal{X} \triangleq \{-2^m + 1, ..., -1, 1, ..., 2^m - 1\}$, where m is the number of bits per symbol. Note that PAS can be readily applied to squared QAM constellations, since a given M-QAM constellation can be seen as the Cartesian product of two $\sqrt{M}$-ASK constellations.

The information binary message $\boldsymbol{u} = (u_1, ..., u_k)$ of length k is uniformly distributed, where $u_i \in \{0, 1\}$. The vector $\boldsymbol{u}$ is split into two vectors $\boldsymbol{u}^{\mathsf{s}}$ and $\boldsymbol{u}^{\mathsf{a}}$, of lengths γn and $k - \gamma n$, respectively, where γ is a design parameter of the PAS. Vector $\boldsymbol{u}^{\mathsf{a}}$ passes a block called distribution matcher to generate a sequence of amplitudes $\boldsymbol{a} = (a_1, ..., a_n)$ with the desired amplitude distribution. The distribution matchers proposed in the literature are mainly classified in two groups, variable-length [113–116] and fixed-length [117]. To limit error propagation, fixed-length distribution matching called *constant composition distribution matching* (CCDM) [117] is employed. Then, the sequence of amplitudes $a_1, ..., a_n$ is transformed into a sequence of bits using the mapper Φ_{ab}. Typically, Φ_{ab} uses Gray mapping (see Sec. 3.2) to reduce the number of bit errors. This leads to a sequence $\boldsymbol{b} = (\boldsymbol{b}_1, \dots, \boldsymbol{b}_n)$ of length $\ell = n(m-1)$ bits. Note that each amplitude can be represented with $m-1$ bits, since one bit is reserved for the corresponding sign. The sequences $\boldsymbol{b}$ and $\boldsymbol{u}^{\mathsf{s}}$ are multiplexed and encoded using a systematic encoder of a linear block code. The rate of the block code is set to $R = \frac{m-1+\gamma}{m}$, hence the sequence of parity bits $\boldsymbol{p} = (\boldsymbol{p}_1, \dots, \boldsymbol{p}_{(1-\gamma)n})$ of length $(1-\gamma)n$ is generated. By multiplexing $\boldsymbol{p}$ and $\boldsymbol{u}^{\mathsf{s}}$, a sequence of bits of length n is constructed. By mapping according to $-1 \mapsto 0$ and $+1 \mapsto 1$, a sequence of sings $s_1, \dots, s_n$ is built. Applying $s_1, \dots, s_n$ to $a_1, ..., a_n$ results in $x_1, \dots, x_n$, as the shaped constellation points. Then, a scaling factor Δ is employed to meet the average power constraint requirement. Finally, the shaped sequence is sent to the channel.

To find the optimal distribution, the Maxwell-Boltzmann distribution given as

$$P_X^{\lambda}(x) = \frac{\exp\left(-\lambda x^2\right)}{\sum_{\tilde{x} \in \mathcal{X}} \exp\left(-\lambda \tilde{x}^2\right)}, \tag{4.1}$$

is typically used, where λ is the so-called shaping parameter. For each SNR, λ is selected such that the corresponding AIR is maximized. The design parameter γ depends on the considered linear code. In [49] LDPC codes are used for encoding, where it is shown that one can operate within 1.1 dB of the capacity of the AWGN channel for a wide range of spectral efficiencies using SDD. In Paper C, we extended

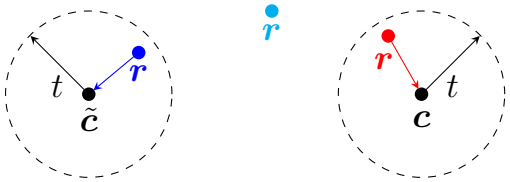

Figure 4.3: The schematic of BDD. The vector $\boldsymbol{c}$ is sent and the decoding is based on the hard detected received vector $\boldsymbol{r}$.

the PAS concept to HDD. In particular, we adopted staircase codes with BCH component codes for PAS. We show that using HDD and shaping, one can operate at a constant gap to the capacity. Furthermore, we show that one can achieve a large range of spectral efficiencies with only a single code, which significantly reduces the decoder complexity. Furthermore, gains up to 2.88 dB with respect to CM with staircase codes and uniform signaling are observed.

4.2 Decoding Techniques for Product-Like Codes

In the previous section, we discussed shaping as a method to improve the performance of a CM system. A complementary approach is to improve the performance of the underlying decoding method. Product-like codes are usually decoded using BDD of the component codes. BDD offers a reasonable performance with a very low decoding complexity. BDD works as follows. Let us assume that the codeword $\boldsymbol{c} = (c_1, \ldots, c_n)$ of length n is transmitted and decoding is based on the hard-detected bits at the channel output, $\boldsymbol{r} = (r_1, \ldots, r_n)$. BDD corrects all error patterns with Hamming weight up to the error-correcting capability of the code t. If the weight of the error pattern is larger than t and there exists another codeword $\tilde{\boldsymbol{c}} \in \mathcal{C}$ with $\mathsf{d_H}(\tilde{\boldsymbol{c}}, \boldsymbol{r}) \leq t$, then BDD erroneously decodes $\boldsymbol{r}$ onto $\tilde{\boldsymbol{c}}$ and a so-called *miscorrection* occurs. Otherwise, if such codeword does not exist, BDD fails and we use the convention that the decoder outputs $\boldsymbol{r}$. Thus, the decoded vector $\hat{\boldsymbol{r}}$ for BDD can be written as

$$\hat{\boldsymbol{r}} = \begin{cases} \boldsymbol{c} & \text{if } \mathsf{d_H}(\boldsymbol{c}, \boldsymbol{r}) \leq t \\ \tilde{\boldsymbol{c}} \in \mathcal{C} & \text{if } \mathsf{d_H}(\boldsymbol{c}, \boldsymbol{r}) > t \text{ and } \exists \tilde{\boldsymbol{c}} \text{ such that } \mathsf{d_H}(\tilde{\boldsymbol{c}}, \boldsymbol{r}) \leq t \\ \boldsymbol{r} & \text{otherwise} \end{cases}. \tag{4.2}$$

In fact, using BDD the decoder only decodes if $\boldsymbol{r}$ is within a sphere of radius t from a codeword. For the sake of illustration, in Fig. 4.3 we show the schematic of BDD. We remark that BDD is an incomplete syndrome decoding where the number of decoded syndromes is limited in order to reduce the decoding complexity. For BCH and RS codes, BDD can be efficiently implemented using the Berlekamp-Massey algorithm. The decoding of product-like codes can then be accomplished in an iterative fashion

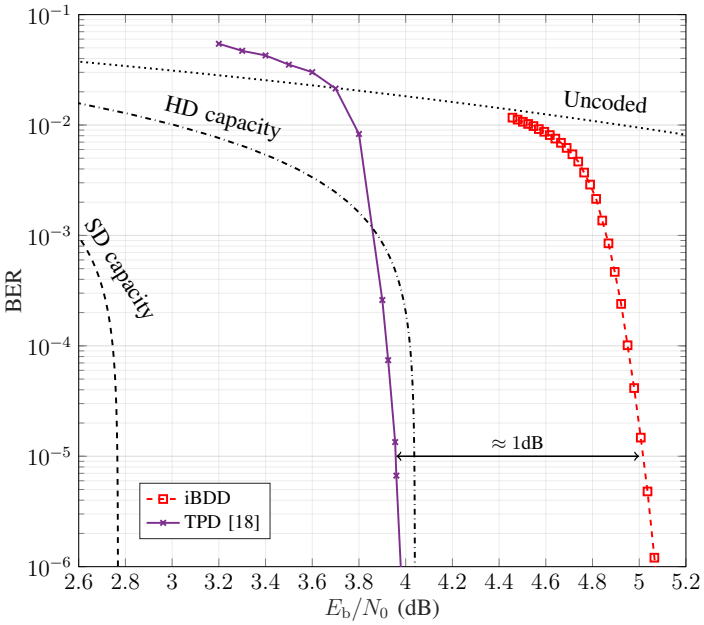

Figure 4.4: Performance comparison of iBDD and TPD based on the Chase-Pyndiah algorithm for a PC with (256,239,6) eBCH component code.

based on the BDD of the component codes. For PCs, one can simply iterate between BDD of row and column codes. Similarly, staircase codes are also decoded using iterative BDD. In particular, decoding is performed in a window-decoding fashion, i.e., the decoder iterates between row and column decoding for the blocks inside a given window for a predefined number of iterations. The size of the window provides a tradeoff between performance and decoding latency, i.e., one expects a performance improvement by increasing the window size at the expense of a higher decoding latency. Here, we refer to iterative decoding of product-like codes based on BDD of the component codes as iterative BDD (iBDD).

The performance of a PC can be improved extensively by employing a more complex decoding algorithm. In particular, turbo product decoding (TPD) based on the Chase-Pyndiah decoding [18], which is an SDD algorithm, allows to operate relatively close to capacity at the cost of significant complexity increase compared to iBDD. In Fig. 4.4, the performance of PCs with extended BCH component code with an OH of 15% is shown for both iBDD and TPD based on the Chase-Pyndiah decoder. Note that iBDD is a HDD algorithm while TPD is an SDD algorithm, hence they have different capacity limits, as shown in Fig. 4.4. As can be seen, there is approximately 1 dB gap between iBDD and TPD. An interesting research question is whether this gap can be reduced by only slightly increasing the decoding complexity. This is a fundamental question that is particularly prominent to address in fiber-optic systems where the complexity of the decoder is an issue, in particular for applications requiring very high throughputs and low power consumption. Recently, have been

some attempts in the literature to address this question.

In [97, 118] a concatenation scheme based on an inner code with SDD and an outer staircase code with HDD was proposed. One can see this proposal as a hybrid of soft and hard decision decoding. The task of the inner code is to reduce the BER to the threshold of the staircase code such that it can reduce the overall BER down to 10^{-15}. In particular, a low-density generator matrix ensemble is considered in [118] for the inner code, while an LDPC code is considered in [97]. The degree distribution of the inner code is designed based on a complexity score to reduce the data flow of the inner code. Interestingly, it is shown that some portion of the inner code bits should be left uncoded, i.e., they are only protected by the outer code [97]. The net coding gains of existing soft-decision FEC designs are achieved with a 56% and 71% reduction in complexity in [118] and [97], respectively.

A new scheme called anchor decoding (AD) was proposed in [119, 120] to reduce the number of miscorrections associated with iBDD for both PCs and staircase codes. The essence of the AD algorithm is based on the observation that in the case of miscorrections, typically two component decoders disagree on the value of a particular bit, leading to a conflict. In conventional iBDD, conflicts are conventionally ignored in the sense that row and column codes are decoded sequentially and previous decoding decisions are simply overridden. The main idea in AD is to introduce status information for each component code and designate certain "reliable" component codes as anchors. The decoder gives more trust on anchors compared to other component codes, e.g., no further additional corrections from other component codes are allowed if this would lead to a conflict and overturn the decision of an anchor. The proposed algorithm also backtracks the decisions of anchors to prevent choosing a miscorrected anchor. This happens whenever too many other component decoders are in conflict with a particular anchor. Pseudocode for AD can be found in [119, Alg. 2]. Overall, it is shown that the gap between conventional iBDD and ideal iBDD where the miscorrections are disregarded using a genie can be reduced with the AD algorithm.

A new decoding algorithm for the decoding of staircase codes has been recently proposed in [121]. The idea is to set less trust on BDD results for code bits corresponding to the last block inside the window decoder. The intuition is that using a window decoder, most of the errors result from the new block in the window. Several checking procedures are proposed to increase the chance of preventing miscorrections. Furthermore, a bit-flipping algorithm is also proposed based on the reliability of the bits to increase the chance of preventing a failure decoding. Overall, gains up to 0.3 dB compared to the base line iBDD are reported.

In Papers D-F, we propose several decoding algorithms to close the gap between SDD and HDD for product-like codes. In particular, an algorithm called iBDD with scaled reliability (iBDD-SR) is proposed in Paper D for both PCs and staircase codes. iBDD-SR exploits the channel reliabilities in order to improve the performance upon iBDD, while keeping the decoding data flow binary (in the sense that only binary

messages are exchanged between the component decoders), as for conventional iBDD. We show that one can roughly achieve the performance of ideal iBDD using iBDD-SR. The beauty of iBDD-SR is that it can be implemented with very low complexity. To verify that, an implementation architecture with 28 nm technology is provided in [52], where we show that PCs with iBDD-SR can achieve the performance of staircase codes under iBDD with less than half area and energy dissipation. In particular, we show that for a PC with 20% OH, 1 Tb/s is achievable with only 0.63 pJ/bit.

In Paper E, we propose an algorithm called iterative generalized minimum distance decoding with scaled reliability (iGMDD-SR) that is based on error and erasure decoding of the component codes. iGMDD-SR brings extra gain compared to iBDD-SR at the cost some extra complexity due to the exchange of soft information between the component decoders. We show that more than 50% of the gap between iBDD and TPD based on the Chase-Pyndiah decoder for PCs can be achieved, with lower complexity compared to TPD.

In Paper F, we propose an algorithm called binary message passing based on GMDD (BMP-GMDD) that can significantly reduce the decoding data flow compared to iGMDD-SR. Interestingly, the performance loss of BMP-GMDD compared to iGMDD-SR is negligible (less than 0.74 dB for the tested PC), hence it provides an excellent performance-complexity tradeoff. Furthermore, BMP-GMDD gives a very limited increase in data flow compared to iBDD. Overall, the schemes proposed in Paper D-F provide flexible choices for the decoding of product-like codes based on a targeted complexity.

Chapter 5

Contributions and Future Work

5.1 Paper A

In Paper A, we analyze the AIRs for CM with HDD. In particular, we assume the conventional HDD where decoding is based on the Hamming distance metric [88–91, 122]. This is the HDD widely used in practice to decode BCH codes and RS codes, as well as PCs and their generalizations. AIRs for CM have been recently analyzed in [94]. However, the decoder referred to as "HDD" in [94] exploits the channel transition probabilities of the discrete memoryless channel (DMC) resulting from the hard detection of the channel output. As such, the "HDD decoder" in [94] exploits soft information and therefore does not fall within the conventional definition of HDD. Furthermore, this is not the HDD used in practice and it is not clear how it can be implemented with low complexity.

In Paper A, we therefore derive the AIRs for the conventional HDD based on the Hamming distance metric for both bit-wise and symbol-wise decoding, corresponding to the use of binary codes (using the BICM paradigm) and nonbinary codes, respectively. An important outcome of this paper is that the AIRs of bit-wise decoders are significantly larger than those of symbol-wise decoders. Therefore, for HDD binary codes are to be preferred for spectrally-efficient fiber-optic communications. This is in sharp contrast with the conclusion in [94], where it was shown that for the decoder that exploits the channel transition probabilities of the DMC, symbol-wise decoding yields higher AIRs. The conclusion arising from our AIRs analysis is confirmed by performance results of binary and nonbinary staircase codes. For nonbinary staircase codes, we derive the DE analysis of the underlying SC-GLDPC code ensemble and optimize the RS code components based on the DE.

5.2 Paper B

In Paper B, we design nonbinary staircase codes with RS codes as component codes. In particular, we consider nonbinary staircase codes as a particular instance of (nonbinary) SC-GLDPC codes. For decoding, we consider the conventional HDD of staircase codes, i.e., iterative BDD based on the Hamming distance metric. We consider the AWGN channel as a proxy of the FOC. With HDD, the AWGN channel (after hard detection) can be modeled as a Q-ary symmetric channel (QSC). We then derive the DE for nonbinary SC-GLDPC codes over the QSC by extending the DE analysis in [101] for SC-GLDPC codes over the binary symmetric channel to the nonbinary case, and optimize the parameters of nonbinary staircase codes based on the DE. By means of simulations, we show that the optimized codes perform best as compared to other nonbinary staircase codes and product codes with the same code rate. The design of nonbinary staircase codes was motivated by the claim in [94] that for HDD symbol-wise decoders achieve larger information rates. However, in Paper A we show that, indeed, for HDD (i.e., the conventional and widely used HDD based on the Hamming distance metric) bit-wise decoders yield higher AIRs. The simulation of binary and nonbinary staircase codes in Paper A confirms this conclusion.

5.3 Paper C

In Paper C, we propose a probabilistic shaping scheme for HDD systems. Motivated by the conclusion driven in Paper A, we consider a bit-wise HDD system. In particular, we extend the PAS concept that was originally proposed in [49] with LDPC codes and SDD to HDD based on staircase codes. To find the optimal distribution, we maximize the AIR of the bit-wise PAS with HDD derived in [123]. We show that using the shaped constellation, one can operate at a constant gap to the capacity of the AWGN channel by changing the modulation order. Then, we design staircase codes with BCH component codes for the PAS architecture. By means of simulations, we show that spectral efficiencies within 0.57–1.44 dB of the AIR are achievable with a fine granularity using only a single staircase code, which reduces the decoding complexity drastically. We also show that PAS with staircase codes outperforms the uniform CM with staircase codes by a large margin. In particular, performance gains up to 2.88 dB are achieved.

5.4 Paper D

Paper D deals with improving the decoding of product-like codes, while keeping the decoding complexity in the same order of conventional iBDD. In particular, a new decoding algorithm called iBDD-SR for the decoding of PCs and staircase codes is proposed. iBDD-SR exploits the channel reliabilities to improve the performance,

while keeping the internal decoder data flow binary, similar to conventional iBDD. In other words, only binary messages are exchanged between the component decoders. In iBDD-SR, we model the decoding failure as erasures, i.e., the corresponding code bit is substituted with the channel output. We consider binary PCs and staircase codes as an instance of (binary) GLDPC and SC-GLDPC code ensembles, and derive a DE to analyze iBDD-SR for GLDPC and SC-GLDPC ensembles. Empowered by the DE analysis, we optimize the design parameter of iBDD-SR for PCs and staircase codes. The derived DE is a generalization of the DE analysis in [124], where the BDD of GLDPC and SC-GLDPC ensembles is analyzed. By means of simulations, we show that iBDD-SR can roughly achieve the performance of the ideal iBDD where the decoder is equipped with a genie to disregard miscorrections. In particular, performance gains up to 0.29 dB and 0.31 dB are achieved compared to the baseline iBDD for PCs and staircase codes, respectively. We also show that iBDD-SR outperforms the AD algorithm [119]. To show the low complexity feature of iBDD-SR, we implemented iBDD-SR in 28 nm technology for PCs in [52]. In particular, we show that PCs with iBDD-SR can achieve similar coding gain as that of staircase codes with iBDD, with only half area and energy dissipation while achieving throughputs up to 1 Tb/s. Furthermore, we show that extra coding gain of iBDD-SR imposes small extra complexity compared to iBDD.

5.5 Paper E

In Paper E, we propose an algorithm, called iGMDD-SR, for iterative decoding of PCs based on GMDD of the component codes. GMDD was originally proposed by Forney [125] for error and erasure decoding of algebraic codes. In GMDD, the least reliable bits are erased and then error and erasure decoding is employed, yielding to a list of candidate codewords. Then, a codeword that minimizes the generalized distance is chosen as the decoding output. GMDD is a soft-input hard-output algorithm, therefore, to be used in our proposed iGMDD-SR, we need to properly define a metric for reliability of the decoded bits. In Paper E, we heuristically model the reliability of the decoded bits as a sum of the channel reliability and scaled GMDD output. To optimize the scaling factors, we perform a Monte-Carlo simulations over a search space where the scaling factor increases over iterations to mimic the reliability improvement of the decoded bits. By means of simulations, we show that iGMDD-SR outperforms iBDD, ideal iBDD, AD, and iBDD-SR. More precisely, iGMDD-SR reduces the gap between iBDD and TPD by more than 50%. We also show that the extra gain of iGMDD-SR over iBDD is at the cost of higher decoding data flow due to exchanging the reliability of bits between component decoders. On the other hand, the complexity of iGMDD-SR is less than that of TPD due to having a smaller list size and relaxing the extrinsic message computation for each code bit.

5.6 Paper F

In Paper F, we propose an algorithm, called BMP-GMDD, for iterative decoding of PCs. BMP-GMDD is a modification of the iGMDD-SR algorithm proposed in Paper E. Similar to iGMDD-SR, BMP-GMDD performs GMDD of the component codes, but at the last stage where GMDD decides for a codeword, the Hamming distance metric instead of the generalized distance metric as in iGMDD-SR is employed. The Hamming distance metric is independent of the reliability of the bits, as opposed to the generalized distance, which requires the reliability of the bits. Therefore, BMP-GMDD requires only the exchange of the indices of the least reliable bits between the component decoders rather than (full soft) reliability of the bits, as required in iGMDD-SR. As a result, the decoder data flow is reduced significantly. By means of simulations, we show that BMP-GMDD outperforms iBDD, ideal iBDD, AD, and iBDD-SR. In particular, the gap between iBDD and TPD is roughly halved using BMP-GMDD. Furthermore, the performance degradation of BMP-GMDD compared to iGMDD-SR is less than 0.1 dB, hence, BMP-GMDD provides an excellent performance–complexity tradeoff. Furthermore, we show that the excellent performance of BMP-GMDD is at the cost of a minor increase in decoder data flow compared to that of iBDD. In particular, we show that the additional data flow of BMP-GMDD compared to iBDD is within the range of 8.5%–34.3%, depending on the code parameters.

5.7 Future Work

In Paper A and Paper B, for the code design, we assumed conventional HDD based on the Hamming distance metric, which effectively transforms the channel into a QSC. This decoding metric does not necessarily give the highest possible AIR. As shown in [94], if the channel transition probabilities of the DMC resulting from the hard detection of the channel output are exploited, higher AIRs can be obtained. Therefore a question arises: is it possible to modify the decoding metric to incorporate these probabilities without increasing the decoding complexity to that of the SDD? Or, is it possible to devise new decoding metrics (not necessarily exploiting the transition probabilities) that yield higher AIRs?

In Paper C, we extended the PAS scheme in [49] to HDD and staircase codes and showed significant gains with respect to the baseline scheme using a uniform constellation. An interesting topic for future work is the analysis of the error floor of the probabilistically-shaped CM scheme in Paper C.

In Paper E and F, we proposed new decoding algorithms for PCs, where the design parameters are selected based on sub-optimal Monte-Carlo simulations. An interesting future work is analyzing iGMDD-SR and BMP-GMDD using the DE framework. This analysis may possibly improve the performance further and will

enhance employing of iGMDD-SR and BMP-GMDD to other product-like codes such as staircase codes.

We expect that Combining the proposed algorithms in Papers D-F with the shaping scheme in Paper C, will provide a powerful CM scheme. An interesting research topic is how close we can operate to the fundamental limit using this approach.

References

[1] R. J. Mears, L. Reekie, I. M. Jauncey, and D. N. Payne, "Low-noise erbium-doped fibre amplifier operating at 1.54μm," *Electronics Lett.*, vol. 23, no. 19, pp. 1026–1028, Sep. 1987.

[2] J. R. S. E. Desurvire and P. C. Becker, "High-gain erbium-doped traveling wave fiber amplifier," *Optics Lett.*, vol. 12, no. 11, pp. 888–890, Nov. 1987.

[3] P. J. Winzer, "Scaling optical fiber networks: Challenges and solutions," *Optics and Photonics News*, vol. 26, no. 3, pp. 28–35, Mar. 2015.

[4] L. Schmalen, A. J. de Lind van Wijngaarden, and S. T. Brink, "Forward error correction in optical core and optical access networks," *Bell Labs Tech. J.*, vol. 18, no. 3, pp. 39–66, Dec. 2013.

[5] C. Shannon, "A mathematical theory of communication," *Bell System Tech. J.*, vol. 27, pp. 379–423, 623–656, Jul./Oct. 1948.

[6] R. Narasimha and N. Shanbhag, "Design of energy-efficient high-speed links via forward error correction," *IEEE Trans. Circ. and Sys. II: Express Briefs*, vol. 57, no. 5, pp. 359–363, May 2010.

[7] B. S. G. Pillai, B. Sedighi, K. Guan, N. P. Anthapadmanabhan, W. Shieh, K. J. Hinton, and R. S. Tucker, "End-to-end energy modeling and analysis of long-haul coherent transmission systems," *IEEE/OSA J. Lightw. Technol.*, vol. 32, no. 18, pp. 3093–3111, Sep. 2014.

[8] B. Sedighi, H. Khodakarami, B. S. G. Pillai, and W. Shieh, "Power-efficiency considerations for adaptive long-haul optical transceivers," *J. Opt. Commun. Netw.*, vol. 6, no. 12, pp. 1093–1103, Dec. 2014.

[9] L. Lundberg, C. Fougstedt, P. Larsson-Edefors, P. A. Andrekson, and M. Karlsson, "Power consumption of a minimal-DSP coherent link with a polarization

multiplexed pilot-tone," in *Proc. Int. Conf. Optical Commun. (ECOC)*, Düsseldorf, Germany, Sep. 2016, pp. 1–3.

[10] M. Kuschnerov, T. Bex, and P. Kainzmaier, "Energy efficient digital signal processing," in *Proc. Optical Fiber Commun. Conf. (OFC)*, San Diego, CA, Mar. 2014, pp. 1–3.

[11] M. Nazarathy and A. Tolmachev, "Efficient DSP methods for coherent optical receiver," in *Proc. Convention of Electrical and Electronics Engineers in Israel*, Israel, Nov. 2012, pp. 1–4.

[12] C. Fougstedt, A. Sheikh, P. Johannisson, A. Graell i Amat, and P. Larsson-Edefors, "Power-efficient time-domain dispersion compensation using optimized FIR filter implementation," in *Proc. Advanced Photonics*, Boston, MA, 2015, p. SpT3D.3.

[13] N. K. Jablon, "Joint blind equalization, carrier recovery and timing recovery for high-order QAM signal constellations," *IEEE Trans. Sig. Processing*, vol. 40, no. 6, pp. 1383–1398, Jun. 1992.

[14] R. Johnson, P. Schniter, T. J. Endres, J. D. Behm, D. R. Brown, and R. A. Casas, "Blind equalization using the constant modulus criterion: a review," *Proc. of the IEEE*, vol. 86, no. 10, pp. 1927–1950, Oct. 1998.

[15] M. J. Ready and R. P. Gooch, "Blind equalization based on radius directed adaptation," in *Proc. Int. Conf. Acoustics, Speech, and Sig. Processing*, Albuquerque, NM, Apr. 1990, pp. 1699–1702.

[16] A. Viterbi, "Nonlinear estimation of PSK-modulated carrier phase with application to burst digital transmission," *IEEE Trans. Inf. Theory*, vol. 29, no. 4, pp. 543–551, Jul. 1983.

[17] D. A. Morero, M. A. Castrillon, F. A. Ramos, T. A. Goette, O. E. Agazzi, and M. R. Hueda, "Non-concatenated FEC codes for ultra-high speed optical transport networks," in *Proc. IEEE Global Telecommun. Conf. (GLOBECOM)*, Houston, TX, Dec. 2011, pp. 1–5.

[18] R. M. Pyndiah, "Near-optimum decoding of product codes: block turbo codes," *IEEE Trans. Commun.*, vol. 46, no. 8, pp. 1003–1010, Aug. 1998.

[19] B. Vasic and I. B. Djordjevic, "Low-density parity check codes for long-haul optical communication systems," *IEEE Photon. Technol. Lett.*, vol. 14, no. 8, pp. 1208–1210, Aug. 2002.

[20] B. Vasic, I. B. Djordjevic, and R. K. Kostuk, "Low-density parity check codes and iterative decoding for long-haul optical communication systems," *IEEE/OSA J. Lightw. Technol.*, vol. 21, no. 2, pp. 438–446, Feb. 2003.

[21] I. Djordjevic, B. Vasic, and R. Kostuk, "Structured LDPC codes for high-speed long-haul optical communications," in *Proc. Optical Fiber Commun. Conf. (OFC)*, Atlanta, GA, Mar. 2003, pp. 393–394.

[22] I. B. Djordjevic, O. Milenkovic, and B. Vasic, "Generalized low-density parity-check codes for optical communication systems," *IEEE/OSA J. Lightw. Technol.*, vol. 23, no. 5, pp. 1939–1946, May 2005.

[23] Z. He, S. Roy, and P. Fortier, "Capacity-approaching LDPC codes with low error floors for high-speed digital communications," in *Biennial Symp. Commun.*, Kigston, Ont., Canada, May 2006, pp. 10–13.

[24] Y. Miyata, K. Kubo, H. Yoshida, and T. Mizuochi, "Proposal for frame structure of optical channel transport unit employing LDPC codes for 100 Gb/s FEC," in *Proc. Optical Fiber Commun. Conf. (OFC)*, San Diego, CA, Mar. 2009, pp. 1–3.

[25] I. B. Djordjevic and B. Vasic, "Nonbinary LDPC codes for optical communication systems," *IEEE Photon. Technol. Lett.*, vol. 17, no. 10, pp. 2224–2226, Oct. 2005.

[26] L. Schmalen, V. Aref, J. Cho, D. Suikat, D. Rösener, and A. Leven, "Spatially coupled soft-decision error correction for future lightwave systems," *IEEE/OSA J. Lightw. Technol.*, vol. 33, no. 5, pp. 1109–1116, Mar. 2015.

[27] C. Häger, A. Graell i Amat, F. Brännström, A. Alvarado, and E. Agrell, "Terminated and tailbiting spatially coupled codes with optimized bit mappings for spectrally efficient fiber-optical systems," *IEEE/OSA J. Lightw. Technol.*, vol. 33, no. 7, pp. 1275–1285, Apr. 2015.

[28] A. Graell i Amat, C. Häger, F. Brännström, and E. Agrell, "Spatially-coupled codes for optical communications: state-of-the-art and open problems," in *Proc. Opto-Electronics and Commun. Conf. (OECC)*, Shanghai, China, Jun. 2015, pp. 1–3.

[29] B. P. Smith, A. Farhood, A. Hunt, F. R. Kschischang, and J. Lodge, "Staircase codes: FEC for 100 Gb/s OTN," *IEEE/OSA J. Lightw. Technol.*, vol. 30, no. 1, pp. 110–117, Jan. 2012.

[30] A. Darabiha, A. C. Carusone, and F. R. Kschischang, "Power reduction techniques for LDPC decoders," *IEEE J. Solid-State Circ.*, vol. 43, no. 8, pp. 1835–1845, Aug. 2008.

References

[31] T. Mohsenin, D. N. Truong, and B. M. Baas, "A low-complexity message-passing algorithm for reduced routing congestion in LDPC decoders," *IEEE Trans. Circ. and Sys. I: Regular Papers*, vol. 57, no. 5, pp. 1048–1061, May 2010.

[32] F. Angarita, J. Valls, V. Almenar, and V. Torres, "Reduced-complexity Min-Sum algorithm for decoding LDPC codes with low Error-Floor," *IEEE Trans. Circ. and Sys. I: Regular Papers*, vol. 61, no. 7, pp. 2150–2158, Jul. 2014.

[33] K. Cushon, P. Larsson-Edefors, and P. Andrekson, "Low-power 400-Gbps soft-decision LDPC FEC for optical transport networks," *IEEE/OSA J. Lightw. Technol.*, vol. 34, no. 18, pp. 4304–4311, Sep. 2016.

[34] International Telecommunication Union, Telecommunication Standardization Sector, "Forward error correction for submarine systems," *ITU-T Rec. G.975*, Nov. 1996.

[35] "Forward error correction for high bit-rate DWDM submarine systems," ITU-T Recommendation G.975.1, 2004.

[36] P. Elias, "Error-free coding," *Trans. IRE Professional Group on Inf. Theory*, vol. 4, no. 4, pp. 29–37, Sep. 1954.

[37] J. Justesen, "Performance of Product Codes and Related Structures with Iterated Decoding," *IEEE Trans. Commun.*, vol. 59, no. 2, pp. 407–415, Feb. 2011.

[38] A. J. Feltstrom, D. Truhachev, M. Lentmaier, and K. S. Zigangirov, "Braided block codes," *IEEE Trans. Inf. Theory*, vol. 55, no. 6, pp. 2640–2658, Jun. 2009.

[39] C. Häger, H. D. Pfister, A. Graell i Amat, and F. Brännström, "Density evolution for deterministic generalized product codes on the binary erasure channel at high rates," *IEEE Trans. Inf. Theory*, vol. 63, no. 7, pp. 4357–4378, Jul. 2017.

[40] L. M. Zhang and F. R. Kschischang, "Staircase codes with 6% to 33% overhead," *IEEE/OSA J. Lightw. Technol.*, vol. 32, no. 10, pp. 1999–2002, May 2014.

[41] C. Häger, A. Graell i Amat, H. D. Pfister, A. Alvarado, F. Brännström, and E. Agrell, "On parameter optimization for staircase codes," in *Proc. Optical Fiber Commun. Conf. (OFC)*, Los Angeles, CA, 2015, pp. 1–3.

[42] M. F. Barsoum, C. Jones, and M. Fitz, "Constellation design via capacity maximization," in *Proc. IEEE Int. Symp. Inf. Theory (ISIT)*, Nice, France, 2007, pp. 1821–1825.

[43] Z. H. Peric, I. B. Djordjevic, S. M. Bogosavljevic, and M. C. Stefanovic, "Design of signal constellations for Gaussian channel by using iterative polar quantization," in *Proc. Mediterranean Electrotechnical Conf., (MELECON)*, vol. 2, Tel-Aviv, Israel, 1998, pp. 866–869.

[44] I. B. Djordjevic, H. G. Batshon, L. Xu, and T. Wang, "Coded polarization-multiplexed iterative polar modulation (PM-IPM) for beyond 400 Gb/s serial optical transmission," in *Proc. Optical Fiber Commun. Conf. (OFC)*, San Diego, CA, 2010, pp. 1–3.

[45] T. Liu and I. B. Djordjevic, "Multidimensional optimal signal constellation sets and symbol mappings for block-interleaved coded-modulation enabling ultrahigh-speed optical transport," *IEEE Photon. J.*, vol. 6, no. 4, pp. 1–14, Aug. 2014.

[46] O. Geller, R. Dar, M. Feder, and M. Shtaif, "A shaping algorithm for mitigating inter-channel nonlinear phase-noise in nonlinear fiber systems," *IEEE/OSA J. Lightw. Technol.*, vol. 34, no. 16, pp. 3884–3889, Aug. 2016.

[47] A. R. Calderbank and L. H. Ozarow, "Nonequiprobable signaling on the gaussian channel," *IEEE Trans. Inf. Theory*, vol. 36, no. 4, pp. 726–740, Jul. 1990.

[48] G. D. Forney, "Trellis shaping," *IEEE Trans. Inf. Theory*, vol. 38, no. 2, pp. 281–300, Mar. 1992.

[49] G. Böcherer, F. Steiner, and P. Schulte, "Bandwidth efficient and rate-matched low-density parity-check coded modulation," *IEEE Trans. Commun.*, vol. 63, no. 12, pp. 4651–4665, Dec. 2015.

[50] E. Berlekamp, "Nonbinary BCH decoding (abstr.)," vol. 14, no. 2, pp. 242–242, Mar. 1968.

[51] J. Massey, "Shift-register synthesis and BCH decoding," *IEEE Trans. Inf. Theory*, vol. 15, no. 1, pp. 122–127, Jan. 1969.

[52] C. Fougstedt, A. Sheikh, A. Graell i Amat, G. Liva, and P. Larsson-Edefors, "Energy-efficient soft-assisted product decoders," in *Proc. Optical Fiber Commun. Conf. (OFC)*, San Diego, CA, 2019.

[53] G. P. Agrawal, *Fiber-optic communication systems.* New York, NY: John Wiley, 2002.

[54] A. Napoli, Z. Maalej, V. A. J. M. Sleiffer, M. Kuschnerov, D. Rafique, E. Timmers, B. Spinnler, T. Rahman, L. D. Coelho, and N. Hanik, "Reduced complexity digital back-propagation methods for optical communication systems," *IEEE/OSA J. Lightw. Technol.*, vol. 32, no. 7, pp. 1351–1362, Apr. 2014.

References

[55] G. P. Agrawal, *Nonlinear fiber optics*. Waltham, MA: Academic Press, Elsevier, 2002.

[56] M. Onishi, Y. Koyano, M. Shigematsu, H. Kanamori, and M. Nishimura, "Dispersion compensating fibre with a high figure of merit of 250 ps/nm/dB," *Electron. Lett.*, vol. 30, no. 2, pp. 161–163, Jan 1994.

[57] E. M. Ip and J. M. Kahn, "Fiber impairment compensation using coherent detection and digital signal processing," *IEEE/OSA J. Lightw. Technol.*, vol. 28, no. 4, pp. 502–519, Feb. 2010.

[58] C. Fougstedt, A. Sheikh, P. Johannisson, and P. Larsson-Edefors, "Filter implementation for power-efficient chromatic dispersion compensation," *IEEE Photon. J.*, vol. 10, no. 4, pp. 1–19, Aug. 2018.

[59] S. J. Savory, "Digital filters for coherent optical receivers," *Opt. Express*, vol. 16, no. 2, pp. 804–817, Jan. 2008.

[60] A. Eghbali, H. Johansson, O. Gustafsson, and S. J. Savory, "Optimal least-squares FIR digital filters for compensation of chromatic dispersion in digital coherent optical receivers," *IEEE/OSA J. Lightw. Technol.*, vol. 32, no. 8, pp. 1449–1456, Apr. 2014.

[61] A. Sheikh, C. Fougstedt, A. Graell i Amat, P. Johannisson, P. Larsson-Edefors, and M. Karlsson, "Dispersion compensation FIR filter with improved robustness to coefficient quantization errors," *IEEE/OSA J. Lightw. Technol.*, vol. 34, no. 22, pp. 5110–5117, Nov. 2016.

[62] C. Häger and H. D. Pfister, "Deep learning of the nonlinear schrödinger equation in fiber-optic communications," in *Proc. IEEE Int. Symp. Inf. Theory (ISIT)*, Vail, CO, Jun. 2018, pp. 1590–1594.

[63] R. A. Fisher and W. K. Bischel, "Numerical studies of the interplay between self-phase modulation and dispersion for intense plane-wave laser pulses," *J. Applied Physics*, vol. 46, no. 4921–4934,, pp. 1–19, 1975.

[64] M. S. O'Sillivan, K. Roberts, and C. Bontu, "Electronic dispersion compensation techniques for optical communication systems," in *Proc. Int. Conf. Optical Commun. (ECOC)*, vol. 2, Glasgow, UK, Sep. 2005, pp. 189–190.

[65] S. J. Savory, "Optimum electronic dispersion compensation strategies for nonlinear transmission," *Electron. Lett.*, vol. 42, no. 7, pp. 407–408, Mar. 2006.

[66] L. Zhu and G. Li, "Nonlinearity compensation using dispersion-folded digital backward propagation," *Opt. Express*, vol. 20, no. 13, pp. 14 362–14 370, Jun 2012.

[67] J. X. Cai, H. Zhang, H. G. Batshon, M. Mazurczyk, O. V. Sinkin, D. G. Foursa, A. N. Pilipetskii, G. Mohs, and N. S. Bergano, "200 Gb/s and dual wavelength 400 Gb/s transmission over transpacific distance at 6.0 b/s/Hz spectral efficiency," *IEEE/OSA J. Lightw. Technol.*, vol. 32, no. 4, pp. 832–839, Feb. 2014.

[68] D. S. Millar, R. Maher, D. Lavery, T. Koike-Akino, M. Pajovic, A. Alvarado, M. Paskov, K. Kojima, K. Parsons, B. C. Thomsen, S. J. Savory, and P. Bayvel, "Design of a 1 Tb/s superchannel coherent receiver," *IEEE/OSA J. Lightw. Technol.*, vol. 34, no. 6, pp. 1453–1463, Mar. 2016.

[69] L. Galdino, M. Tan, A. Alvarado, D. Lavery, P. Rosa, R. Maher, J. D. Ania-Castanon, P. Harper, S. Makovejs, B. C. Thomsen, and P. Bayvel, "Amplification schemes and multi-channel DBP for unrepeatered transmission," *IEEE/OSA J. Lightw. Technol.*, vol. 34, no. 9, pp. 2221–2227, May 2016.

[70] N. V. Irukulapati, H. Wymeersch, P. Johannisson, and E. Agrell, "Stochastic digital backpropagation," *IEEE Trans. Commun.*, vol. 62, no. 11, pp. 3956–3968, Nov. 2014.

[71] N. V. Irukulapati, D. Marsella, P. Johannisson, E. Agrell, M. Secondini, and H. Wymeersch, "Stochastic digital backpropagation with residual memory compensation," *IEEE/OSA J. Lightw. Technol.*, vol. 34, no. 2, pp. 566–572, Jan. 2016.

[72] C. Häger and H. D. Pfister, "Wideband Time-Domain digital backpropagation via subband processing and deep learning," in *Proc. Int. Conf. Optical Commun. (ECOC)*, Rome, Italy, Sep. 2018, pp. 1–3.

[73] C. K. A. Splett and K. Petermann, "Ultimate transmission capacity of amplified optical fiber communication systems taking into account fiber nonlinearities," *Proc. Int. Conf. Optical Commun. (ECOC)*, Sep. 1993.

[74] V. Curri, P. Poggiolini, A. Carena, and F. Forghieri, "Dispersion compensation and mitigation of nonlinear effects in 111-Gb/s WDM coherent PM-QPSK systems," *IEEE Photon. Technol. Lett.*, vol. 20, no. 17, pp. 1473–1475, Sep. 2008.

[75] E. Torrengo, R. Cigliutti, G. Bosco, A. Carena, V. Curri, P. Poggiolini, A. Nespola, D. Zeolla, and F. Forghieri, "Experimental validation of an analytical model for nonlinear propagation in uncompensated optical links," in *Proc. Int. Conf. Optical Commun. (ECOC)*, Geneva, Switzerland, 2011, pp. 1–3.

[76] G. Bosco, R. Cigliutti, A. Nespola, A. Carena, V. Curri, F. Forghieri, Y. Yamamoto, T. Sasaki, Y. Jiang, and P. Poggiolini, "Experimental investigation

of nonlinear interference accumulation in uncompensated links," *IEEE Photon. Technol. Lett.*, vol. 24, no. 14, pp. 1230–1232, Jul. 2012.

[77] A. Nespola, S. Straullu, A. Carena, G. Bosco, R. Cigliutti, V. Curri, P. Poggiolini, M. Hirano, Y. Yamamoto, T. Sasaki, J. Bauwelinck, K. Verheyen, and F. Forghieri, "Extensive fiber comparison and GN-model validation in uncompensated links using DAC-generated Nyquist-WDM PM-16QAM channels," in *Proc. Optical Fiber Commun. Conf. (OFC)*, Anaheim, CA, Mar. 2013, pp. 1–3.

[78] P. Poggiolini, "The GN model of non-linear propagation in uncompensated coherent optical systems," *IEEE/OSA J. Lightw. Technol.*, vol. 30, no. 24, pp. 3857–3879, Dec. 2012.

[79] L. Beygi, E. Agrell, P. Johannisson, M. Karlsson, and H. Wymeersch, "A discrete-time model for uncompensated single-channel fiber-optical links," *IEEE Trans. Commun.*, vol. 60, no. 11, pp. 3440–3450, Nov. 2012.

[80] A. Carena, V. Curri, G. Bosco, P. Poggiolini, and F. Forghieri, "Modeling of the impact of nonlinear propagation effects in uncompensated optical coherent transmission links," *IEEE/OSA J. Lightw. Technol.*, vol. 30, no. 10, pp. 1524–1539, May 2012.

[81] P. Johannisson and E. Agrell, "Modeling of nonlinear signal distortion in fiber-optic networks," *IEEE/OSA J. Lightw. Technol.*, vol. 32, no. 23, pp. 3942–3950, Dec. 2014.

[82] A. Carena, G. Bosco, V. Curri, Y. Jiang, P. Poggiolini, and F. Forghieri, "EGN model of non-linear fiber propagation," *Opt. Express*, vol. 22, no. 13, pp. 16 335–16 362, Jun. 2014.

[83] G. Ungerboeck and I. Csajka, "Codes correcteurs d'erreurs," vol. 2, pp. 147–156, 1959.

[84] G. Ungerboeck, "Channel coding with multilevel phase signals," *IEEE Trans. Inf. Theory*, vol. 28, no. 1, pp. 55–67, Jan. 1982.

[85] H. Imai and S. Hirakawa, "A new multilevel coding method using error-correcting codes," *IEEE Trans. Inf. Theory*, vol. 23, no. 3, pp. 371–377, May 1977.

[86] A. Bennatan and D. Burshtein, "Design and analysis of nonbinary LDPC codes for arbitrary discrete-memoryless channels," *IEEE Trans. Inf. Theory*, vol. 52, no. 2, pp. 549–583, Feb. 2006.

[87] E. Zehavi, "8-PSK trellis codes for a Rayleigh channel," *IEEE Trans. Commun.*, vol. 40, no. 5, pp. 873–884, May 1992.

[88] A. Lapidoth, *A foundation in digital communication.* Cambridge, UK: Cambridge University Press, 2009.

[89] A. Barg, "Complexity issues in coding theory," *Handbook of Coding Theory*, vol. I, V.S. Pless, W.C. Huffman, Editors, North Holland, 2007.

[90] V. Guruswami, *List decoding of error-correcting codes.* Springer Science & Business Media, 2004.

[91] A. Vardy, "Algorithmic complexity in coding theory and the minimum distance problem," in *Proc. Annual ACM Symp. Theory of Computing*, El Paso, TX, May 1997, pp. 92–109.

[92] N. Merhav, G. Kaplan, A. Lapidoth, and S. Shamai (Shitz), "On information rates for mismatched decoders," *IEEE Trans. Inf. Theory*, vol. 40, no. 6, pp. 1953–1967, Nov. 1994.

[93] J. Scarlett, A. Martinez, and A. Guillén i Fàbregas, "Mismatched decoding: Error exponents, second-order rates and saddlepoint approximations," *IEEE Trans. Inf. Theory*, vol. 60, no. 5, pp. 2647–2666, May 2014.

[94] G. Liga, A. Alvarado, E. Agrell, and P. Bayvel, "Information rates of next-generation long-haul optical fiber systems using coded modulation," *IEEE/OSA J. Lightw. Technol.*, vol. 35, no. 1, pp. 113–123, Jan. 2017.

[95] E. Berlekamp, *Algebraic Coding Theory.* McGraw-Hill, New York, 1968.

[96] T. M. Cover and J. A. Thomas, *Elements of Information Theory.* Wiley-Interscience, 1991.

[97] M. Barakatain and F. R. Kschischang, "Low-complexity concatenated LDPC-Staircase codes," *IEEE/OSA J. Lightw. Technol.*, vol. 36, no. 12, pp. 2443–2449, Jun. 2018.

[98] R. C. Bose and D. K. Ray-Chaudhuri, "On a class of error correcting binary group codes," *Inform. Control*, vol. 3, no. 1, pp. 68–79, Mar. 1960.

[99] I. S. Reed and G. Solomon, "Polynomial codes over certain finite fields," *J. Soc. Indust. App. Math.*, vol. 8, no. 2, pp. 300–304, Jun. 1960.

[100] N. Abramson, "Cascade decoding of cyclic product codes," *IEEE Trans. Commun. Tech.*, vol. 16, no. 3, pp. 398–402, Jun. 1968.

[101] Y.-Y. Jian, H. D. Pfister, K. R. Narayanan, R. Rao, and R. Mazahreh, "Iterative hard-decision decoding of braided BCH codes for high-speed optical communication," in *Proc. IEEE Global Telecom. Conf. (GLOBECOM)*, Atlanta, GA, Dec. 2013.

[102] Z. Qu and I. B. Djordjevic, "Geometrically shaped 16QAM outperforming probabilistically shaped 16QAM," in *Proc. Int. Conf. Optical Commun. (ECOC)*, Gothenburg, Sweden, Sep. 2017, pp. 1–3.

[103] B. Chen, C. Okonkwo, D. Lavery, and A. Alvarado, "Geometrically-shaped 64-point constellations via achievable information rates," in *Int. Conf. Transparent Optical Networks (ICTON)*, Bucharest, Romania, Jul. 2018, pp. 1–4.

[104] E. Sillekens, D. Semrau, D. Lavery, P. Bayvel, and R. I. Killey, "Experimental demonstration of geometrically-shaped constellations tailored to the nonlinear fibre channel," in *Proc. Int. Conf. Optical Commun. (ECOC)*, Rome, Italy, Sep. 2018, pp. 1–3.

[105] F. Steiner and G. Böcherer, "Comparison of geometric and probabilistic shaping with application to ATSC 3.0," in *Proc. Int. Conf. on Source and Channel Coding (SCC)*, Hamburg, Germany, Feb. 2017.

[106] C. Pan and F. R. Kschischang, "Probabilistic 16-QAM shaping in WDM systems," *IEEE/OSA J. Lightw. Technol.*, vol. 34, no. 18, pp. 4285–4292, Sep. 2016.

[107] T. Fehenberger, A. Alvarado, G. Böcherer, and N. Hanik, "On probabilistic shaping of quadrature amplitude modulation for the nonlinear fiber channel," *IEEE/OSA J. Lightw. Technol.*, vol. 34, no. 21, pp. 5063–5073, Nov. 2016.

[108] T. Yoshida, M. Karlsson, and E. Agrell, "Performance metrics for systems with soft-decision FEC and probabilistic shaping," *IEEE Photon. Technol. Lett.*, vol. 29, no. 23, pp. 2111–2114, Dec. 2017.

[109] G. Böcherer, F. Steiner, and P. Schulte, "Fast probabilistic shaping implementation for long-haul fiber-optic communication systems," in *Proc. Int. Conf. Optical Commun. (ECOC)*, Gothenburg, Sweden, Sep. 2017, pp. 1–3.

[110] G. Böcherer, "On joint design of probabilistic shaping and forward error correction for optical systems," in *Proc. Optical Fiber Commun. Conf. (OFC)*, San Diego, CA, Mar. 2018, pp. 1–36.

[111] T. Fehenberger, G. Böcherer, A. Alvarado, and N. Hanik, "LDPC coded modulation with probabilistic shaping for optical fiber systems," in *Proc. Optical Fiber Commun. Conf. (OFC)*, Los Angeles, CA, Mar. 2015, pp. 1–3.

[112] Z. Qu and I. B. Djordjevic, "Optimal constellation shaping in optical communication systems," in *Int. Conf. Transparent Optical Networks (ICTON)*, Bucharest, Romania, Jul. 2018, pp. 1–5.

[113] F. R. Kschischang and S. Pasupathy, "Optimal nonuniform signaling for Gaussian channels," *IEEE Trans. Inf. Theory*, vol. 39, no. 3, pp. 913–929, May 1993.

[114] G. Böcherer and R. Mathar, "Matching dyadic distributions to channels," in *Proc. Data Compression Conf. (DCC)*, Snowbird, UT, Mar. 2011, pp. 23–32.

[115] S. Baur and G. Böcherer, "Arithmetic distribution matching," in *Proc. Int. Conf. Sys., Commun. and Coding (SCC)*, Hamburg, Germany, Hamburg, 2015, pp. 1–6.

[116] R. A. Amjad and Böcherer, "Fixed-to-variable length distribution matching," in *Proc. IEEE Int. Symp. Inf. Theory (ISIT)*, Istanbul, Turkey, 2013, pp. 1511–1515.

[117] P. Schulte and Böcherer, "Constant composition distribution matching," *IEEE Trans. Inf. Theory*, vol. 62, no. 1, pp. 430–434, Jan. 2016.

[118] L. M. Zhang and F. R. Kschischang, "Low-complexity soft-decision concatenated LDGM-Staircase FEC for high-bit-rate fiber-optic communication," *IEEE/OSA J. Lightw. Technol.*, vol. 35, no. 18, pp. 3991–3999, Sep. 2017.

[119] C. Häger and H. D. Pfister, "Approaching miscorrection-free performance of product codes with anchor decoding," *IEEE Trans. Commun.*, vol. 66, no. 7, pp. 2797–2808, Jul. 2018.

[120] ——, "Miscorrection-free decoding of staircase codes," in *Proc. Int. Conf. Optical Commun. (ECOC)*, Gothenburg, Sweden, Sep. 2017, pp. 1–3.

[121] Y. Lei, A. Alvarado, B. Chen, X. Deng, Z. Cao, J. Li, and K. Xu, "Decoding staircase codes with marked bits," in *Proc. Int. Symp. Turbo Codes & Iterative Inf. Processing (ISTC)*, Hong Kong, Dec. 2018, pp. 1–5.

[122] S. Lin and D. J. Costello Jr., *Error Control Coding, Second Edition.* Upper Saddle River, NJ: Prentice-Hall, Inc., 2004.

[123] G. Böcherer, "Achievable rates for probabilistic shaping." [Online]. Available: http://arxiv.org/abs/arXiv:1707.01134.

[124] Y. Jian, H. D. Pfister, and K. R. Narayanan, "Approaching capacity at high rates with iterative hard-decision decoding," *IEEE Trans. Inf. Theory*, vol. 63, no. 9, pp. 5752–5773, Sep 2017.

[125] G. Forney, "Generalized minimum distance decoding," *IEEE Trans. Inf. Theory*, vol. 12, no. 2, pp. 125–131, Apr. 1966.